Early-life stress impairs development of functional interactions and neuronal activity within prefrontal-amygdala networks *in vivo*

Angelica Donati, M.Sc.[a] (angelica.donati@helsinki.fi),

Francescangelo Vedele, Ph.D.[a,b] (francescangelo.vedele@helsinki.fi),

Henrike Hartung, Ph.D.[a#] (henrike.hartung@helsinki.fi)

corresponding author

a HiLIFE Neuroscience Center, P.O. 63, FI-00014 University of Helsinki, Helsinki, Finland
b Department of Physiology, Medicum, University of Helsinki, Helsinki, Finland.

Abstract

Early-life stress (ELS), such as parental neglect or abuse, predisposes an individual to develop mental disorders. Disease hallmarks include heightened amygdala reactivity and impaired prefrontal cortex-amygdala functional interactions, already during childhood and adolescence. However, which cellular and circuit mechanisms underlie these hallmarks, as well as the altered developmental trajectory of prefrontal-amygdala networks, is poorly understood. Here we performed simultaneous *in vivo* local-field potential and multi-unit recordings under light urethane anaesthesia in the medial prefrontal cortex (mPFC) and basolateral amygdala (BLA) of male and female pre-juvenile or adolescent mice, exposed to a resource scarcity model of ELS. We find a developmentally transient low-theta (3-5 Hz) oscillatory hypercoupling within mPFC-BLA networks in pre-juvenile ELS males which seems to result from a precocious development of coupling strength after ELS. In the mPFC, neuronal spiking activity was decreased in pre-juvenile males and the local theta entrainment of spike firing disrupted. In BLA, both sexes showed an increase in firing activity in a subpopulation of neurons after ELS, also confirmed by an increase in ΔFosB-positive neurons in BLA, which we identified to be non-GABAergic. Directed interactions, i.e. the ability to entrain spike firing in mPFC to the theta rhythm in BLA and vice versa, were also impaired predominantly in pre-juvenile males after ELS, while females showed a milder phenotype. These early sex-dependent impairments in the functional development of prefrontal-amygdala circuits may promote aberrant development of emotional behaviours after ELS and may predispose to a disease phenotype later on.

40 **1. Introduction**

41 Early-life stress (ELS) such as parental neglect, maltreatment, or abuse, is a strong risk factor for
42 depression and anxiety disorders [1-3]. Studies in humans and animal models have pointed to
43 malfunction of prefrontal-amygdala networks as the substrate increasing the risk for psychiatric
44 symptoms after the experience of ELS [4, 5]. Both the amygdala and the prefrontal cortex are
45 particularly vulnerable to early stressors due to their protracted postnatal development. Most
46 extensively for the amygdala, but also for other limbic brain regions, it has been shown that ELS
47 leads to an accelerated structural and functional maturation across species, i.e. a precocious
48 development of emotion circuits [6]. The most consistent findings among individuals with a history of
49 ELS are amygdala hyper-reactivity to (mainly) negative emotional cues as well as impaired prefrontal
50 cortex-amygdala task-elicited or resting-state functional connectivity detected as early as childhood
51 [4, 5]. How these ELS hallmarks emerge and determine each other, particularly concerning the
52 protracted and sequential development of this circuit, is still hardly understood.

53 The recently developed limited bedding and nesting (LBN) model mimics resource scarcity and
54 altered parental care, which is often related to early adversity in humans [7, 8]. The altered rearing
55 condition induces stress to the dam and leads to unpredictable maternal care patterns [7-9]. Mice
56 reared under LBN conditions display delayed physical growth and deficits in spatial [10, 11] and
57 contextual learning [12, 13] as well as depressive-like behaviours [14] and increased anxiety [15] in a sex-
58 dependent manner. Furthermore, hyper-reactivity of amygdala networks, as measured by a
59 stimulus-induced increase in the immediate early gene cFos-positive neurons in the basolateral
60 amygdala (BLA), has also been found in this model[, 17]. *In vitro* electrophysiological recordings after
61 ELS showed increased excitatory input to BLA neurons and increased synaptic plasticity (LTP) [18, 19]
62 predominantly in males, but also an increase in the intrinsic excitability of BLA neurons likely
63 mediated by reduced expression of SK channels [20]. However, how ELS affects neuronal spiking
64 activity within prefrontal-amygdala networks *in vivo* is still largely unknown. In line with data in
65 humans, ELS rodent models also show impaired prefrontal-amygdala functional connectivity as
66 measured by fMRI or tractography predominantly in males, that strongly correlate with behavioural
67 impairments in innate anxiety or fear conditioning [15, 21-26]. However, direct electrophysiological

measurements of how ELS affects the development of local prefrontal or amygdala network activity and their long-range interactions remain sparse.

Here, we used a cumulative combination of the LBN resource scarcity model and maternal separation (MS) to investigate the effect of ELS on *in vivo* network activity, as well as long-range functional interactions between prelimbic (PL) or infralimbic (IL) subdivisions of the medial prefrontal cortex (mPFC) and BLA during pre-juvenile (postnatal day (P) 18-20) or adolescent (P43-47) development in male and female pups. Cumulative ELS exposure to LBN+MS has previously been shown to lead to an anxiety phenotype in male mice as well as aberrant prefrontal-amygdala functional and structural connectivity [15, 24]. Besides, initial behavioural characterization of our cumulative ELS model during adulthood also revealed increased anxiety-like behaviours in ELS males and strong deficits in classical fear conditioning in both ELS males and females[27]. In this study, we found functional impairments within prefrontal-amygdala networks after ELS already during pre-juvenile development predominantly in males, such as oscillatory hypercoupling in the low-theta band (3-5 Hz) as well as disrupted directed interactions within prelimbic-BLA networks. Moreover, in the mPFC neuronal spiking activity was decreased, and local theta entrainment was disrupted in ELS males. In contrast, in pre-juvenile BLA, a subpopulation of presumably principal neurons showed increased firing activity after ELS in both sexes. This effect was even more prominent during adolescent development with a broad increase in mean firing rates in ELS males. This study is one of the first investigating the impact of ELS on the functional development of prefrontal-amygdala networks by direct *in vivo* electrophysiological measurements. Our data provide further evidence for pre-juvenile development as a susceptible period following ELS, during which both an impairment in functional long-range interactions as well as an abnormal local neuronal firing activity emerge in the PL and in the BLA. These early impairments may lead to major circuit dysfunction underlying disease in adulthood.

2.2 Materials and Methods

2.1 Animals

95 Experiments were performed using male and female C57Bl/6J mice. All experiments were done in
96 accordance with the University of Helsinki Animal Welfare Guidelines and approved by the Animal
97 Experiment Board in Finland (license ESAVI/13422/2018 and ESAVI/27422/2022). Mice were
98 maintained on a 12-hour light-dark cycle (lights on from 6 am to 6 pm) with *ad libitum* access to food
99 and water. Mice were housed in a quiet room adjacent to the laboratory to minimize stress from
100 transportation.

101 **2.2 Early-life stress protocol (limited bedding and nesting + maternal separation)**

102 The limited bedding and nesting (LBN) protocol was a modified version of the protocol used by KG
103 Bath and co-workers, see [28]. In total 48 litters between 4-8 pups including at least two pups of each
104 sex were randomly assigned to either control or LBN group. The average litter size was similar in
105 both experimental groups (control: 6.0 ± 1.2 pups/litter, LBN: 6.2 ± 1.3 pups/litter). At P4, the dam
106 and the entire litter were transferred to a cage with a wire mesh floor (L30cm x W30cm x H1cm) 1
107 cm above the cage floor and half a nestlet (2,3 x 5 cm) as the only source of nesting material. Food
108 and water were supplied *ad libitum*. The LBN dam and litter remained in these housing conditions
109 until P14. In this study, the LBN period was extended to include the developmental time window
110 (P10-14) during which prefrontal cortical projections to BLA steeply increase [29, 30]. In addition, pups
111 were separated from their dams for 1 h on P8, P10, and P12 by moving the whole litter to a standard
112 cage with normal bedding and nesting material, placed on a heating pad to maintain body
113 temperature. Otherwise, the dam and pups were left undisturbed. Pups were weighed individually at
114 P14 upon return to a standard home cage and were weaned at P21. Control litters were housed in
115 standard home cages (L 42 cm x W 25 cm x H 15 cm) with a normal supply of bedding and nesting
116 material as well as *ad libitum* access to food and water, and were left undisturbed between P4-14
117 and weaned at P21.

118 **2.3 *In vivo* electrophysiology**

119 *Surgical preparation.* Extracellular recordings were performed in the mPFC and in the anterior part
120 of the BLA (BLAa) of P18-20 (pre-juvenile) and P43-47 (adolescent) male and female mice.

121 Pups were weighed and anaesthesia was induced with isoflurane (5%) followed by i.p. administration
122 of urethane (1.2 g/kg; Sigma-Aldrich, USA). Isoflurane administration (1-2%) continued during
123 surgery to ensure deep anaesthesia. An incision along the midline was made and the skull was
124 exposed. Small burr holes were drilled above the regions of interest (mPFC: 1.2-1.3 mm anterior to
125 bregma and 0.1 mm from the midline, BLA: 1.5-1.7 posterior to Bregma, at the base of the rhinal
126 fissure) in the right hemisphere, and the bone was carefully removed to prevent tissue damage and
127 bleeding. The head of the pup was fixed into the stereotaxic apparatus (RWD Life Science, China)
128 using two hollow plastic bars fixed with dental cement on the nasal and occipital bones. The body
129 temperature was maintained at 37 °C with a thermoregulated heating blanket (Supertech
130 Instruments, UK). A urethane top-up of 1/5 of the original dose was administered if needed.
131 Multielectrode arrays (32-channel, four-shank (4x8) silicon Michigan probes (0.4 -2 MΩ), A4x8-5mm-
132 200-200-177-A32 (mPFC) or A4x8-5mm-100-200-177 (BLAa), NeuroNexus Technologies, USA)
133 were inserted perpendicular to the skull surface into the mPFC until a depth of 1.8-2.0 mm, and at
134 40° from the vertical plane into the BLAa at a depth of 2.0-2.2 mm. The distance between shanks
135 was 200 µm and the recording sites were separated by 100 µm (BLAa) or 200 µm (mPFC). The
136 electrodes were labelled with DiI (1,1'-dioctadecyl-3,3,3',3'-tetramethyl indocarbocyanine,
137 Invitrogen, USA) to enable reconstruction of the electrode tracks postmortem (Figure 1B). A silver
138 wire was inserted into the cerebellum and served as common ground and reference electrode.

139 *Recording protocol.* After a 20-25 min recovery period, simultaneous recordings of local field
140 potential (LFP) and multi-unit activity (MUA) were performed from PL and IL subregions of the mPFC
141 and the BLAa. The position of recording sites over PL, IL, and BLAa was confirmed by post-mortem
142 histological evaluation. Both LFP and MUA were recorded at a sampling rate of 32 or 30 kHz using
143 a multi-channel extracellular amplifier (Digital Lynx 4SX, Neuralynx, USA or Open Ephys acquisition
144 board, Open Ephys, USA) and their corresponding acquisition software. During recording the signal
145 was band-pass filtered between 0.1 Hz and 8 kHz (Neuralynx) or 0.1 Hz and 7.9 kHz (Open Ephys).

146 *Perfusion/Fixation.* After the recording, pups received another dose of more concentrated urethane
147 (2g/kg) for deep surgical anaesthesia and were perfused with 0.1 M PBS followed by 4%

148 paraformaldehyde (PFA). Brains were postfixed in 4% PFA for a further 48 h. Free-floating 70 µm
149 coronal sections containing mPFC and BLAa were cut on a vibratome (Leica VT 1200S, Leica
150 Biosystems, USA) and mounted onto adhesive slides (SuperFrost Plus, VWR, USA). Sections
151 containing the labelled electrode tracts were imaged using brightfield microscopy (Olympus BX61,
152 Olympus, Japan) and a 1,25x objective connected to a camera (Olympus DP73, Olympus, Japan).

153 *Data analysis.* Channels for analysis were selected on the basis of post-mortem histological
154 investigation, i.e. which recording sites of fluorescently-marked electrodes were confined to PL, IL,
155 and BLAa (n = 182 animals in total). A matching atlas plate from the adult mouse Allen Brain
156 Reference Atlas (Allen Mouse Brain Atlas, atlas.brain-map.org) was superimposed at a similar
157 rostral-caudal level on the brightfield photomicrograph image to determine which recording
158 electrodes were located within the regions of interest (Figure 1B). Of those, individual channels with
159 best signal-to-noise ratio over superficial layers II/II or deep layers V/VI of PL or IL, and medial
160 aspects of predominantly BLAa were analysed according to the anatomical development of this
161 projection [28]. Recordings where the electrode placement was outside the areas of interest, or
162 showing prominent heartbeat or noise artifacts, were excluded from further analysis. Data were
163 imported and analysed off-line using custom-written MATLAB scripts (v. R2023a, MathWorks, USA).
164 The signals were low-pass filtered (<1000 Hz) using a third-order Butterworth filter before
165 downsampling to 2000 Hz. An IIR notch filter was applied at 50 Hz to attenuate line noise. All data
166 analyses were performed blind to the group belonging of the pup.

167 *Spectral analysis.* The power spectral density (PSD) was estimated using Welch's method (MATLAB
168 function "*pwelch*") and a sliding window approach (10-s Hamming window, 50% overlap).

169 *Coherence analysis.* To measure spectral correlation between signals in the mPFC and BLAa,
170 magnitude-squared coherence (MSC) was calculated with the MATALB function *mscohere*. MSC is
171 defined as a function of the PSD of each signal ($P_{xx}(f)$ *and* $P_{yy}(f)$, where x and y represent signals
172 from different areas), and the cross power spectral density $P_{xy}(f)$, formally related as ***Equation 1***.
173 Data was bandpass-filtered between 0-100 Hz and divided into 3-second windows with 50% overlap
174 for this analysis. Confidence intervals were determined by repeating MSC calculation between a 3-

second window in one area, shuffled with a Monte Carlo simulation (100 iterations per window), and the corresponding original window in the other area. The analysis was repeated for all windows initially used for the calculation of the MSC, and the 95th percentile of the resulting distribution was used as confidence limit. To compare the coherence between groups, the area under the curve in the band of interest (low-theta, 3-5 Hz) was calculated for each experiment with trapezoidal numerical integration.

Spike sorting. All channels within PL, IL or BLAa containing spiking activity were imported into the Offline Sorter^{TM} software (Plexon) to sort MUA into single units. First, the data was high-pass filtered (>400 Hz) using a 2nd order Butterworth filter. Then, spikes were detected by using amplitude threshold that was set manually after visual inspection, and the spike timestamp was defined as the largest amplitude event within each electrode. The detected spikes were automatically sorted into individual units using the Valley Seeking or K-means method. The Valley Seeking method applies an algorithm to inter-point distances to detect the number of clusters and cluster membership. The K-means method is an iterative algorithm that assigns the waveforms to one of the user-indicated cluster centres, based on Euclidean distance in feature space. Units with a signal-to-noise ratio (SNR) below 5 for OpenEphys recordings or below 11 for Neuralynx recordings were excluded. Individual spiking units were identified if their corresponding spike clusters were clearly separated in feature space (Isolation Distance > 25 and L-Ratio < 0.5), the waveform shape was consistent with a clear resemblance to derivatives of action potentials and the interspike interval (ISI) histogram showed a refractory period of > 1 ms (Plexon Offline Sorter). If a unit occurred simultaneously in more than one channel, it was included only in the channel with the highest SNR, to prevent double counting.

Analysis of single unit firing activity. The mean firing rate of each unit (number of spikes/s) and the Fano factor (variance of number of spikes/average of number of spikes) were calculated in MATLAB using the exported spike timestamps from the Plexon Offline Sorter.

Sorting of units into putative excitatory regular spiking vs putative inhibitory fast-spiking. To sort the recorded units into putative excitatory vs putative inhibitory, we used the spike waveforms and

202 plotted the valley to peak latency as a function of the half-width (see scatter plots in Suppl. Fig. 6A),
203 as previously used in the developing mPFC [31, 32]. Regular spiking vs fast spiking units were
204 distinguished by setting a manual threshold (half-width < 0.3 ms, valley-to-peak time < 0.3 ms).

205 *Phaselocking analysis*. To study spike-field synchronization (i.e. locking of spike time to LFP phase),
206 we used the LFP Analysis toolbox (Beteje toolbox by Jelfs, https://github.com/beteje/LFP_Analysis,
207)[33], along with custom-written MATLAB scripts (available upon request). Single-unit spike
208 timestamps obtained with Plexon were imported into MATLAB, along with the corresponding LFP
209 filtered between 0-100 Hz. The phase of the LFP at each spike time was estimated with a continuous
210 wavelet transform (Morlet, 4 cycles) for 5 frequencies between 3 and 5 Hz, in 0.5 Hz intervals. Phase
211 0° corresponded to the peak of the oscillation, whereas phase ±180° to the through of the oscillation.
212 To verify whether a unit was significantly phase-locked to the LFP, a Raileigh test with a threshold
213 of 0.05 with Bonferroni correction based on the number of frequencies analysed (p = 0.05/5 = 0.01)
214 was performed. A unit was deemed to be locked to the LFP if a significant Bonferroni-corrected p
215 value was obtained for at least one frequency in the 3-5 Hz range. The preferred phase angle for
216 each group was calculated as the circular mean, in degrees, of the significantly locked units, using
217 the CircStat toolbox in MATLAB [33]. The difference in the average phase angle between groups was
218 measured with the Watson-William test. The difference in distribution between locked and non-
219 locked units between groups was evaluated with the Fisher's test.

220 **2.4 Analysis of ΔFosB-positive neurons in BLA**

221 *Tissue preparation.* Male and female control and ELS mice were sacrificed at two different time
222 points, at P14, immediately after the LBN treatment, and at P18, corresponding to the time of the *in*
223 *vivo* electrophysiological recordings (control: P14, male: N= 5, female: N= 5, P18, male: N= 5,
224 female: N = 4, from 7 litters in total; ELS: P14, male: N = 5, female: N = 3, P18, male: N = 5, female:
225 N = 4, from 4 litters in total). Mice were deeply anesthetized with urethane (2g/kg, Sigma-Aldrich,
226 USA) and were intracardially perfused with 4% PFA in 0.1 M PBS for 20 minutes. Following
227 perfusion, brains were extracted and stored in 4% PFA for 48 h at 4°C. Then, brains were washed
228 with 0.1 M PBS and free-floating 30 µm coronal sections containing BLAa were cut on a vibratome

229 (Leica VT 1200S, Leica Biosystems, USA). Sections were stored in anti-freeze solution (30%
230 ethylene glycol, 30% glycerol, 30% distilled water and 10% 0.244 M phosphate buffer 2xPO_4) at -
231 20°C for further processing.

232 *Immunohistochemistry.* Brain sections were washed for 5 x 7 min in PBS + 0.1 % Triton X-100 (PBS-
233 T) and incubated in blocking solution (PBS-T + 5% donkey serum) for 2 h at room temperature (RT).
234 Next, sections were incubated in PBS-T containing the primary antibodies (see Table 1) overnight
235 at 4°C. Then, after washing 3 x 15 min in PBS-T, the sections were incubated for 2 h at RT in PBS-
236 T containing the secondary antibodies. Finally, sections were washed 3 x 15 min in PBS-T and
237 mounted using Fluoromount-G™ mounting medium with DAPI (Thermo Fisher).

Immunogen	Dilution	Host	Manufacturer	ID
PanFosB (FosB/ΔFosB)	1:300	Mouse	Abcam	Ab11959
FosB	1:300	Rabbit	Thermo Fisher	PA5-79280
GAD67/GAD1	1:1000	Goat	Abcam	Ab80589
Mouse-488	1:2000	Donkey	Abcam	Ab150105
Rabbit-568	1:2000	Donkey	Abcam	Ab175470
Goat-647	1:1000	Donkey	Abcam	Ab150131

238 **Table 1.** Primary and secondary antibodies used in this study.

239 *Light microscopy imaging.* Light microscopy images from four brain sections/animal containing BLAa
240 were obtained with the Zeiss Axio Imager M2 microscope equipped with an Apotome 2 structured
241 illumination microscopy (SIM) slider, using Plan Apo 20x (NA = 0.8) objective (Zeiss, Oberkochen,
242 Germany), fitted with a Hamamatsu ORCA Flash 4.0 V2 camera (Hamamatsu Photonics K.K.,
243 Japan). The ZEN 2 software (Zeiss) was used for image acquisition.

244 *Image analysis.* To estimate the density of ΔFosB immunopositive (+) cells in the BLA, images with
245 merged channels for FosB and PanFosB (FosB/ΔFosB) were analysed using ImageJ Fiji software.
246 $FosB^+$ cells as well as FosB/PanFosB double positive neurons were excluded and only the remaining

247 PanFosB$^+$ within the boundaries of BLAa were manually counted, as only those expressed the Δ
248 splice variant of FosB. To quantify the intensity of the ΔFosB fluorescent signal, the difference
249 between the single cell signal and the section's background was determined. The quantification was
250 then normalized to the average intensity values measured in controls [35]. The density estimation of
251 GAD67$^+$ cells and the quantification of the GAD67 signal intensity were conducted using the same
252 methods.

253 **2.5 Statistical analysis**

254 All statistical analyses were done on raw data using Prism, version 9.4.0 (GraphPad, USA), custom-
255 written MATLAB scripts, or MATLAB community toolboxes. The sample size was based on previous
256 experience on similar experiments. The distribution of the data was tested with the D'Agostino-
257 Pearson test, and two-sided parametric (unpaired t-test, Welch´s t-test) or non-parametric tests
258 (Mann-Whitney U test) were chosen accordingly. Uniformity of circular data was measured with the
259 Rayleigh test. Differences between groups in circular data were evaluated with the Watson-Williams
260 test. To measure the relative effect of the LBN treatment onto any outcome along the two time points
261 (P18-20 and P43-47), a two-way ANOVA was used, with post-hoc Sidák correction for multiple
262 comparisons. The results were considered significant when $p < 0.05$. All the pooled data are given
263 as mean ± SEM or or mean ± SD or median (interquartile range (IQR)) as noted. In the figures,
264 statistical significance levels are indicated by asterisks as follows: *p < 0.05, **p < 0.01, ***p < 0.001,
265 and ****p < 0.0001.

266

267 **3. Results**

268 **3.1 ELS does not affect the development of local oscillatory network activity in mPFC or BLAa**

269 To test the effect of ELS on the development of prefrontal-amygdala networks, male and female
270 pups were exposed to the ELS LBN paradigm between P4-14 with additional MS for 1 h at P8, P10,
271 and P12 (Fig. 1A). This combined treatment of LBN+MS has been shown to result in an amygdala
272 phenotype before [15]. Previous studies characterizing the LBN model have shown a consistent

decrease in physical growth i.e. body weight or body weight gain of LBN pups compared to controls [12, 14, 36]. Similarly, we also found a significant decrease in body weight in ELS males of 19.87 ± 1.69 % at the end of the LBN treatment period (P14, Suppl. Fig. 1Ai), which slowly recovered to 12.84 ± 1.62 % during pre-juvenile (P18-21) development and to 6.48 ± 2.40 % during adolescence (P43-47, Two-Way ANOVA, factor treatment: $F(2, 179) = 35.00$, $p < 0.0001$, factor age: $F(2, 179) = 1936$, $p < 0.0001$, n = 18-46 pups/group, Sidak's multiple comparisons tests: P14, $p < 0.0001$; P18, $p = 0.025$; P45, $p = 0.0025$). ELS females also showed a significant decrease in body weight at P14 (13.79 ± 2.30 %, Suppl. Fig. 1Aii), as well as during pre-juvenile (10.88 ± 1.73 %) and adolescent development (6.44 ± 1.42 %, Two-Way ANOVA, factor treatment: $F(2, 174) = 30.19$, $p < 0.0001$, factor age: $F(2, 174) = 1871$, $p < 0.0001$, n = 24-45 pups/group, Sidak's multiple comparisons tests: P14, $p = 0.024$; P18, $p = 0.0085$; P45, $p = 0.0005$). Hence, we are confident that our implementation of the LBN ELS paradigm was successful.

Following the ELS paradigm, spontaneous local-field potential (LFP) and multi-unit activity (MUA) within superficial (II/III) or deep (V/VI) layers of the right PL or IL cortex (Fig. 1Bi, Suppl. Fig. 1Bi) or the BLAa (Fig. 1Bii, Suppl. Fig. 1Bii) were recorded from pre-juvenile (P18-20) or adolescent (P43-47) male and female ELS pups under light urethane anaesthesia as well as from control pups at the same age.

Spontaneous prefrontal network activity in control male and female pre-juvenile mice (Fig. 1Ci, Di, Supp. Fig. 1Ci) was continuous and was characterized by prominent high-amplitude delta rhythms (0.3-0.5 Hz) superimposed by theta, most prominent low-theta (3-6 Hz), beta and gamma (12-100 Hz) activity as well as local MUA, as typical for urethane-induced slow-wave sleep-like activity [37-39]. During adolescent development (Fig. 1Cii), high-amplitude delta activity became faster (peak frequency ~1 Hz) and particularly the superimposed low-theta activity (3-6 Hz) was even more prominent, evident as clear peaks in the related power spectra (Fig. 1Dii). Network activity was similar between PL and IL (Fig. 1D, Suppl. Fig. 1C) and between superficial and deep cortical layers within either developmental period. No differences were found between males and females at either

age. Furthermore, cortical network activity in ELS mice was also not significantly different from controls in neither males nor females at either developmental time point (Fig 1D).

Spontaneous network activity in pre-juvenile BLAa was also characterized by high-amplitude delta activity (0.3-0.5 Hz) with superimposed prominent theta activity, particularly low-theta (3-6 Hz), as well as beta and gamma activity and MUA (Fig. 1Ei, Fi). Similarly to cortical network activity, during adolescent development delta rhythms became faster (~ 1 Hz, Fig. 1Eii) and low-theta activity increased in power, as it can be seen by the prominent peaks (3-6 Hz) in the power spectrum (Fig. 1Fii). Network activity in the BLAa was similar between males and females at either developmental time point. Moreover, BLAa network activity was also not significantly different between ELS and control mice neither during pre-juvenile nor during adolescent development (Fig. 1F).

Hence, it seems that ELS does not affect the generation of neither cortical nor amygdala spontaneous network activity per se during neither pre-juvenile nor adolescent development.

3.2. ELS impairs prefrontal-amygdala oscillatory coupling during pre-juvenile development in males only

ELS has been shown to impair functional interactions within developing prefrontal-amygdala networks [15, 21-26]. However, most of the data was obtained by resting-state fMRI and electrophysiological investigations in mouse models of ELS remain sparse. Our previous study in pre-pre-juvenile (P14-15) ELS rats exposed to daily maternal separation between P2-14 revealed a decrease in oscillatory coupling within prefrontal-amygdala networks in the low-theta range (2-5 Hz) in males only [26]. To investigate if sex-dependent impairments in functional coupling within prefrontal-amygdala networks particularly in low-theta range is a general signature of ELS across different species and ELS models, we analysed coherence as a measure of coupling synchrony in pre-juvenile and adolescent control and ELS male and female mice. Generally, coherence in the 0-40 Hz range was significantly larger compared to shuffled data within both prelimbic superficial layers-BLAa or prelimbic deep layers-BLAa in pre-juvenile males and females (Fig. 2A), and the same was true for coherence within pre-juvenile infralimbic-BLAa networks (Suppl. Fig. 2). Since our previous

325 study in developing rats identified low-theta as a substrate for prefrontal-amygdala interactions [26],
326 we focussed our coherence analysis on the low-theta range (3-5 Hz) as well. Coherence within either
327 prelimbic superficial layers-BLAa or prelimbic deep layers-BLAa networks showed a broad peak in
328 low-theta range (3-5 Hz) in both pre-juvenile control male and female pups (Fig. 2A). In ELS mice,
329 this peak in low-theta range was even more prominent in both pre-juvenile males and females.
330 However, when comparing the area under the curve (AUC) from 3-5 Hz between treatment groups,
331 low-theta coherence was selectively increased versus controls only within prelimbic superficial
332 layers- BLAa networks and only in pre-juvenile males (Fig. 2B, $t(21) = 2.297$, $p = 0.032$, N = 11-12,
333 unpaired t-test). In contrast, no significant changes in low-theta coherence were observed in pre-
334 juvenile ELS females. Furthermore, when analysing low-theta coherence within infralimbic-BLAa
335 networks (Suppl. Fig. 2), no significant changes were observed neither within infralimbic superficial
336 layers-BLAa nor within infralimbic deep layers-BLAa networks, in neither pre-juvenile ELS males nor
337 females versus controls.

338 Hence, ELS selectively impairs long-range functional interactions within pre-juvenile prelimbic
339 superficial layers-BLAa networks in a sex-dependent manner only in males while females were not
340 significantly affected.

341 **3.3. Prefrontal-amygdala oscillatory coupling is not affected during adolescent development**

342 To assess if the impairments in functional long-range interactions within prelimbic-amygdala
343 networks persist into adolescence, we computed coherence within prelimbic-BLAa or infralimbic-
344 BLAa networks in adolescent male and female mice. Again, we focussed our analysis on oscillatory
345 coupling within low-theta (3-5 Hz) range. Control adolescent male and female mice showed
346 prominent peaks in low-theta coherence within prelimbic superficial layers-BLAa or prelimbic deep
347 layers-BLAa (Fig. 3A, B). However, to our surprise the pre-juvenile hypercoupling within prelimbic
348 superficial layers-BLAa was not present anymore in adolescent ELS males, and low-theta coherence
349 within this network was similar to control males. Likewise, ELS did not affect low-theta coherence
350 within prelimbic superficial layers-BLAa in adolescent females. Also, low-theta coherence within
351 prelimbic deep layers-BLAa was similar between control and ELS mice in both males and females.

Coherence within infralimbic superficial layers-BLAa or infralimbic deep layers-BLAa also showed prominent peaks within low-theta range (Suppl. Fig. 3A, B) in both male and female adolescent control mice. ELS did not affect low-theta coherence within infralimbic-BLAa networks either. Low-theta coherence in adolescent ELS males or females within infralimbic superficial layers-BLAa or infralimbic deep layers-BLAa was not significantly different from controls.

Hence, during adolescence, spontaneous oscillatory coupling within prelimbic-BLAa or infralimbic BLAa networks was not affected by ELS in neither male nor female mice.

3.4 ELS mice show a smaller developmental increase in mPFC-amygdala coherence indicating a precocious development in coupling strength

It has been shown both in humans with a history of ELS and in rodent models that ELS causes a precocious development of amygdala networks as well as prefrontal-amygdala structural and functional connectivity [6, 25, 40]. Here we analysed if ELS also has an effect on the developmental increase in oscillatory coupling within prefrontal-amygdala networks. Generally, coherence across 0-40 Hz Hz within both prelimbic-BLAa (Fig. 3C, D) or infralimbic-BLAa (Suppl. Fig. 3C, D) networks was higher in adolescent versus pre-juvenile mice. When calculating the fold-change in low-theta coherence between pre-juvenile and adolescent mice, low-theta coherence increased by 3.7 (1.2) fold within prelimbic superficial layers-BLAa or 2.5 (1.8) fold within prelimbic deep layers-BLAa in control males. This change was significantly smaller in ELS mice, with only a 1.8 (1.6) fold increase in coherence within prelimbic superficial layers-BLAa ($t(19) = 4.76$, $p = 0.0001$, N = 9-12, unpaired t-test) or a 1.7 (1.2) fold increase in coherence within prelimbic deep layers-BLAa ($t(22) = 2.55$, $p = 0.018$, N = 11-13, unpaired t-test). In control females, low-theta coherence increased by 2.1 (1.8) fold within prelimbic superficial layers-BLAa or by 2.2 (1.2) fold within prelimbic deep layers-BLAa. Similar to ELS males, the increase in low-theta coherence was significantly smaller in ELS females and increased only by 1.9 (1.1) fold within prelimbic superficial layers-BLAa ($t(24) = 2.25$, $p = 0.034$, N = 11-15, unpaired t-test) or by 1.6 (0.7) fold within prelimbic deep layers-BLAa ($t(28) = 3.55$, $p = 0.0014$, N = 13-17, unpaired t-test). Also, infralimbic-amygdala low-theta coherence was higher in adolescent vs pre-juvenile mice across the 0-40 Hz spectrum (Suppl. Fig. 3C, D). Low-theta

379 coherence increased by 3.1 (0.5) fold within infralimbic superficial layers-BLAa or by 2.8 (1.2) fold
380 within infralimbic deep layers-BLAa in control males. Interestingly, ELS only led to a significant
381 decrease in this change, suggesting a precocious development within infralimbic superficial layers-
382 BLAa (ELS: 2.1 (1.2), U = 19, p = 0.035, N = 9-10, Mann-Whitney test) but not within infralimbic deep
383 layers-BLAa in male mice. In control females, low-theta coherence increased by 2.2 (1.3) fold within
384 infralimbic superficial layers-BLAa or 2.3 (1.7) fold within infralimbic deep layers-BLAa. Remarkably,
385 the increase in theta coupling within infralimbic-amygdala networks across development was not
386 affected by ELS.

387 Accordingly, the largest difference between control and ELS mice regarding the increase in low-theta
388 coupling was within prelimbic superficial layers-BLAa in males (Fig, 3Ci) due to the particularly strong
389 increase in theta coupling within controls across development, as well as the prominent low-theta
390 hypercoupling within this network in pre-juvenile ELS males. Hence, the increase in low-theta
391 coherence across development was particularly diminished within prelimbic-amygdala networks in
392 both ELS males and females. This may indicate that ELS causes a precocious development in
393 functional long-range interactions predominantly within prelimbic-amygdala networks in this ELS
394 mouse model.

395 **3.5 ELS leads to a higher firing activity of a subpopulation of units in pre-juvenile BLAa and**
396 **to a widespread increase in firing activity in adolescent BLAa**

397 One of the hallmark signatures of ELS in humans is an increased amygdala reactivity [4, 41]. Previous
398 work in mouse models of ELS also suggested an increased activity of BLA neurons based on cFos
399 analysis [, 17]. Here, we analysed the firing activity in BLAa in male and female control and ELS mice.
400 For this, MUA was sorted into single units using the Plexon Offline Sorter. In pre-juvenile control
401 males, n = 41 BLAa single units from N = 12 mice were obtained. Their firing rates were low 0.62
402 (1.34) Hz and the Fano factor, a measure for the variability of neural spike trains, was 1.86 (1.00)
403 suggesting that spiking patterns were irregular and variable over time (Fig. 4A). In pre-juvenile ELS
404 males, n = 36 single BLAa units from N = 12 mice were obtained. Their firing rates (0.68 (1.95)) and
405 Fano factors (1.83 (1.03)) were similar to controls (Fig. 4A). However, when plotting the logarithmic

frequency distribution of firing rates (Fig. 4B), control mice showed a unimodal distribution while ELS mice showed a bimodal distribution of firing rates. This suggests that in controls the data was obtained from a single, similarly active population of neurons. Interestingly, the bimodal distribution in ELS mice indicates two distinct populations of neurons, one firing at higher rates than the other. We did not find any anti-correlation between firing rate and half-width (Suppl. Fig. 4Ai) which would have been expected if the more active population of neurons after ELS were fast-spiking interneurons. Clustering using similar criteria as for the mPFC (see below) did not reveal more than one cluster per group, which were also overlapping (Suppl. Fig. 4Aii). Hence, this suggests that increased neuronal activity in the BLAa after ELS is due to activation of a subpopulation of principal neurons rather than increased population activity of fast-spiking interneurons. Finally, we also analysed and compared the spike waveforms in both groups. The valley-to-peak time (ms) of the spikes, corresponding to the duration of the medium afterhyperpolarization (mAHP) of the extracellular action potential, was significantly decreased in ELS males versus control males (Fig. 4Ci, control: 0.40 (0.1), ELS: 0.32 (0.1), $t(75) = 4.262$, $p < 0.0001$, $n = 36\text{-}41$, unpaired t-test). This suggests a significantly shorter mAHP in the spikes of ELS mice, which is a typical indicator of increased excitability [42]. When computing the full width at half maximum (FWHM) of the waveform (see diagram in Fig. 4Ci), the duration in control and ELS mice was similar (Fig. 4Cii), suggesting, in line with our results from clustering, recordings were sampled from similar types of neurons in both groups, most likely predominantly BLAa principal neurons.

In pre-juvenile females, after spike sorting n = 34 BLAa single units from N = 9 control mice and n = 24 BLAa single units from N = 10 ELS mice were obtained. As in control males, baseline firing rates in the BLAa in control females (Fig. 4D) were also low (0.69 (2.41) Hz) and had a similar Fano factor (1.96 (1.22)). Furthermore, neither baseline firing rates (0.78 (1.67) Hz) nor Fano factor (1.78 (1.26)) in ELS females were significantly different from controls. However, when plotting the logarithmic frequency distribution of firing rates in both groups (Fig. 4E), similar to males, control females showed a unimodal distribution while ELS females showed a bimodal distribution of firing rates. This suggests that also in females, the data was obtained from a single similarly active population of

433 neurons in controls, but from two separate populations in ELS mice, one with higher firing activity.
434 Again, when clustering the spikes as for males above (Suppl. Fig. 4B), we did not find any evidence
435 that more active neurons would be putative fast-spiking interneurons. Hence, the more active
436 population of BLA neurons after ELS are most likely also BLA principal neurons. When computing
437 the valley-to-peak time (ms) or the FWHM of BLAa spike waveforms (Fig. 4F), no differences were
438 observed between control and ELS females. This suggests that in contrast to pre-juvenile ELS
439 males, in ELS females the intrinsic excitability of BLAa neurons was not altered by ELS, but, as in
440 males, active neurons in both groups seem to belong to similar types of cells, i.e. most likely BLAa
441 principal neurons.

442 Next, we performed spike sorting and analysed neuronal firing activity in BLAa of adolescent control
443 and ELS mice. We obtained n = 47 single units from N = 10 adolescent control males and n = 77
444 single units from N = 11 adolescent ELS males. Remarkably, adolescent ELS males showed a
445 significant increase in mean baseline firing rates compared to controls (Fig. 4G(i), control: 0.71 (1.2)
446 Hz, ELS: 1.64 (3.2) Hz, U = 1130, p = 0.0004, Mann-Whiteny test). Moreover, the Fano factor was
447 also significantly increased in adolescent ELS males compared to controls. (Fig. 4G(ii), control: 1.53
448 (0.7), ELS: 1.84 (0.7), U = 1229, p = 0.0028, Mann-Whitney test). These data show that ELS not
449 only leads to a prominent increase in baseline firing activity in males but also affects the firing
450 patterns. The logarithmic frequency distribution of firing rates showed a unimodal distribution for both
451 adolescent male control and ELS mice (Fig. 4H). while ELS mice exhibited a skewness towards
452 higher firing rates in accordance with the increased firing rate (Fig. 4H). The change from a bi-modal
453 distribution in prejuvenile ELS males to a unimodal distribution of firing rates in adolescent ELS
454 males suggests a more widespread increase in firing activity affecting a larger population of BLAa
455 neurons in adolescent ELS males. Similar to pre-juvenile development, we did not find any anti-
456 correlation between firing rate and half-width (Suppl. Fig. 4Ci) and clustering also only revealed one
457 larger cluster in each treatment group which were overlapping (Suppl. Fig. 4Cii). This suggests that
458 increased neuronal activity in BLAa of adolescent ELS males is due to activation of predominantly
459 on large population of neurons, proabably BLAa principal neurons. Interestingly, valley-to-peak time

of the spike was not significantly different between the groups (Fig. 4I(i)), while FWHM was decreased in adolescent ELS males compared to controls (Fig. 4I(ii), $t(122) = 2.93$, $p = 0.0041$, N = 47-77, unpaired t-test).

In BLAa of adolescent females, we obtained n = 109 BLAa single units from N = 14 control and n = 29 single units from N = 8 ELS mice. In contrast to males at the same age, firing rates were not significantly increased after ELS (Fig. 4 J(i)), but the Fano factor was strongly increased (Fig. 4J(ii), control: 1.91 (0.9), ELS: 3.22 (2.5), $U = 746$, $p < 0.0001$, Mann-Whitney test). However, there was a trend towards increased firing rates (control: 1.22 (1.8), ELS: 1.70 (2.8), $U = 1257$, $p = 0.0913$, Mann-Whitney test) as well in adolescent ELS females that probably did not reach significance due to the lower number of units in this group. The logarithmic frequency distribution of firing rates showed a unimodal distribution for adolescent female controls (Fig. 4K) while the distribution remained inconclusive in adolescent ELS females due to the low number of units in this group. Both valley-to-peak time of the spike (Fig. 4 L(i), control: 0.54 (0.1), ELS: 0.52 (0.05), $U = 1145$, $p = 0.0225$) and FWHM (Fig. 4L(ii), $t(136) = 3.50$, $p = 0.0006$, unpaired t-test) were significantly decreased in adolescent ELS females compared to controls, pointing to an overall shorter duration of the action potential in this group.

Hence, while during pre-juvenile development neither the mean firing rates nor the firing patterns seem to be affected in BLAa by ELS, in both pre-juvenile ELS males and females a subpopulation of BLA neurons showed higher firing activity. Furthermore, only in pre-juvenile ELS males this was accompanied by changes in the spike waveform, suggesting an increased intrinsic excitability. During adolescent development, this phenotype was even stronger showing a prominent increase in mean firing rates in BLAa in ELS males while this effect did not reach significance in females probably due to the lower number of units. Moreover, also the firing patterns were impaired in both sexes after ELS whereas modifications in action potential shape point to altered membrane excitability or ion channel expression after ELS.

486 **3.6 ELS leads to persistent activation of pre-juvenile BLA neurons in both males and females**

487 To confirm the findings from our *in vivo* recordings, we carried out immunohistochemistry against
488 ΔFosB, a marker of chronic activation in neurons [43], in the BLAa (Fig. 5). Since no antibodies against
489 ΔFosB were available, we performed dual-immunolabelling against PanFosB, which labels both
490 FosB and ΔFosB immunopositive (+) neurons and FosB. Those PanFosB$^+$ neurons that did not
491 colocalize with FosB were counted as ΔFosB$^+$ (see Fig. 5A). Data were collected at P14, immediately
492 after the LBN stress period, and during pre-juvenile development at P18, at the same age when the
493 *in vivo* electrophysiological recordings were carried out. In males, two-way ANOVA revealed a
494 significant effect of ELS treatment ($F(1, 16) = 4.757$, $p = 0.044$, N = 5 mice/group) but no effect of
495 age nor of the age x ELS treatment interaction on the number of BLAa ΔFosB$^+$ cells (Fig. 5Bi, Suppl.
496 table 4) suggesting that ELS leads to an increase in the number of ΔFosB$^+$ neurons in the BLAa in
497 males that is independent of age. When analysing the data separately for either right or left
498 hemisphere in both groups at both ages (Fig. 5Bii), there was still a significant effect of ELS treatment
499 (three-way ANOVA, $F(1, 29) = 6.718$, $p = 0.0148$) on the number of ΔFosB$^+$ neurons, but no effect
500 of neither hemisphere nor age, nor any significant interactions (hemisphere x age, hemisphere x
501 ELS treatment, age x ELS treatment, hemisphere x age x ELS treatment in males, (Suppl. table 4).
502 We also determined the intensity of the ΔFosB signal as a percentage of control, but did not find any
503 significant effects of neither ELS treatment nor age nor ELS treatment x age interaction (Fig. 5Biii,
504 Suppl. table 4).

505 Interestingly, the effects of ELS in females were even stronger (Fig. 5Ci). There was a significant
506 effect of ELS treatment on the number of BLAa ΔFosB$^+$ neurons (Two-way ANOVA, $F(1, 12) = 6.992$,
507 $p = 0.0214$, N = 3-5 mice/group, Suppl. table 4) and also a significant effect of age ($F(1, 12 = 17.79$,
508 $p = 0.0012$) as well as an ELS treatment x age interaction ($F(1, 12) = 9.132$, $p = 0.0106$). In addition,
509 post-hoc tests revealed a significant increase in the number of ΔFosB$^+$ neurons induced by ELS
510 treatment at P18 ($p = 0.0031$) but not at P14. Hence, in females ELS leads to an age-dependent
511 increase in the number of ΔFosB+ neurons in the BLAa during pre-juvenile development at P18-20.

512 When analysing the data separately for left and right hemispheres (Fig. 5Cii), similar to males, there
513 was no effect of the hemisphere, but still an effect of ELS treatment (Three-way ANOVA, $F(1, 22) =$
514 10.67, $p = 0.0035$, Suppl. table 4) and age ($F(1, 22) = 17.98$, $p = 0.0003$) as well as ELS treatment
515 x age interaction ($F(1, 22) = 10.54$, $p = 0.0037$). Finally, when determining the intensity of the ΔFosB
516 signal as a percentage of control (Fig. 5Ciii), there was no effect of ELS treatment and neither of age
517 nor ELS treatment x age interaction (Suppl. table 4).

518 Hence, while ELS leads to an age-independent increase in the number of ΔFosB$^+$ neurons in the
519 BLAa in males, in females ELS leads to an age-dependent increase in the number of ΔFosB$^+$ neurons
520 in the BLAa specifically during pre-juvenile development. In both males and females the effect was
521 similar in either hemisphere and the intensity of the signal did not change neither with age nor with
522 ELS treatment. These data further support the results from the *in vivo* electrophysiological recordings
523 in the BLAa, and strongly indicate persistent activation of a population of BLAa neurons by ELS in
524 both males and females during pre-juvenile development.

525 **3.7 ELS persistently activates non-GABAergic neurons in pre-juvenile BLAa**

526 It has previously been shown that GABAergic interneurons in the BLA, particularly parvalbumin (PV)
527 interneurons, are highly susceptible to ELS, as they show precocious maturation resulting in
528 increased numbers during pre-juvenile development following ELS [12, 44]. Moreover, their synaptic
529 and structural input is also affected by ELS, leading to altered feed-forward inhibition in the
530 developing amygdala [26]. To investigate whether those BLAa neurons showing increased activity after
531 ELS as determined by ΔFosB$^+$ immunohistochemistry are also GABAergic, we performed triple
532 immunohistochemistry against FosB, PanFosB and the 67 dDa isoform of the GABA synthesizing
533 enzyme glutamate decarboxylase (GAD67) (Fig. 6) in P18 control and ELS mice. As above (see Fig.
534 5), PanFosB$^+$ neurons that did not co-localize with FosB were identified as ΔFosB$^+$. To limit the
535 number of animals needed, we conducted these experiments with remaining tissue generated for
536 the experiments described in Figure 5. The data show a similar trend of increased ΔFosB$^+$ neurons
537 after ELS (Fig. 6Bi), but did not quite reach statistical significance. However, the number of GAD67$^+$

538 neurons was similar in all four experimental groups (Fig. 6Bii) as was the intensity of the staining
539 which was clearly distinct from background (Suppl. Fig. 5). Interestingly, in neither control nor ELS
540 males, ΔFosB$^+$ neurons co-localized with GAD67$^+$ neurons at all (0%, Fig. 6A(i), B(iii)), suggesting
541 that they are rather glutamatergic projection neurons. In females though, ΔFosB$^+$ neurons co-
542 localized with GAD67$^+$ neurons in a low percentage of cells in controls (4 ± 2.72 %) which was similar
543 after ELS (5 ± 5.42 %) (Fig. 6Aii, Biii). There was high variability between mice as half of the controls
544 and 3/4 ELS females showed no co-localization, while 7% or 11% of co-localization was observed
545 in the remaining two control females vs 22% of co-localization in the remaining ELS female.

546 Hence, these data strongly suggest that ELS leads to a persistent activation of predominantly BLAa
547 principal neurons rather than GABAergic interneurons. Whether in females ELS also leads to an
548 activation of GABAergic neurons in the BLAa still has to be determined in a larger dataset.

549 **3.8 ELS leads to a lower firing activity of neurons in the prefrontal cortex of pre-juvenile males**

550 To get a better understanding of how ELS affects the development of the pre-juvenile mPFC, we
551 sorted cortical MUA into single units and analysed their firing activity. We focussed our analysis on
552 superficial layers II/III within PL due to its strong connectivity with BLAa [45, 46]. In control males, we
553 obtained n = 54 units from N = 11 pups and in ELS males n = 90 units from N = 13 pups. Baseline
554 firing rates in control PL were low (1.45 (1.68) Hz) and Fano factor was 1.80 (1.27) indicating high
555 variability in the firing activity (Fig. 7A). Interestingly, baseline firing rates in the PL of ELS mice were
556 significantly lower than in controls (0.89 (1.37) Hz, U = 1902, p = 0.029, Mann-Whitney test) but the
557 Fano factor was similar (1.76 (0.96)). We also analysed the spike waveforms in both groups (Fig.
558 7B). Both valley-to-peak time (ms) and FWHM were similar between control and ELS males. The
559 decrease in neuronal firing activity within the PL of ELS males may be due to a change in the
560 excitation/inhibition balance or an increased feed-forward inhibition. We relied on the shape of the
561 extracellular waveform to sort all recorded PL units into putative regular spiking excitatory vs putative
562 fast-spiking inhibitory units as previously shown for spiking activity in the pre-juvenile PFC [32] (Suppl.
563 Fig. 6Ai). Interestingly, the ratio of putative inhibitory vs excitatory neurons in the PL was significantly
564 different after ELS (p = 0.0531, Fisher's test). In control males, only one unit (1/54, 2%) was classified

565 as fast-spiking while in ELS males 10 units (10/90, 11%) were classified as fast-spiking. Increased
566 population activity of inhibitory fast-spiking interneurons may contribute to lower baseline firing rates
567 within PL in ELS males. However, immunolabelling against parvalbumin (PV) and subsequent
568 quantification of the density of PV-positive (PV+) neurons in P18 males did not reveal any signifcant
569 differences between control and ELS mice (Suppl. Fig. 8). Thus, it seems that ELS does not lead to
570 higher density of PV+-neurons in BLAa during pre-juvenile development, but rather to an increase
571 in activity of a similar number of PV+ interneurons compared to controls. Moreover, when analysing
572 firing activity within layers V/VI of the IL cortex, which also shows strong connectivity to the BLA [45,
573 46], we also found a decrease in the main firing rates in ELS males (Suppl. Fig. 6B, U = 5527, p =
574 0.0081, Mann-Whitney test). While the ratio of putative excitatory vs inhibitory units was not different
575 between control and ELS mice (Suppl. Fig. 6D), spikes recorded in the IL of ELS mice had a
576 significantly shorter half-width than in controls (Suppl. Fig. 6C, U = 5328, p = 0.0025, Mann-Whitney
577 test), which may also indicate that more putative inhibitory units with faster action potentials are
578 active after ELS in the IL in males.

579 In females, after spike sorting we obtained n = 73 units in N = 13 pups in control and n = 49 units
580 from N = 10 ELS pups. Similar to males, firing rates of PL units in female control mice were low (1.28
581 (1.74) Hz) and Fano factor was 1.50 (0.81), the latter indicating a high variability in firing activity over
582 time (Fig. 7C). Both the firing rate (0.87 (2.03) Hz) of PL units as well as the Fano factor (1.59 (1.26))
583 were similar in ELS mice. Furthermore, the ratio of putative regular spiking excitatory neurons vs
584 putative fast-spiking inhibitory neurons was also similar between the groups (Suppl. Fig. 6Aii). When
585 analysing the valley-to-peak time (ms) of the PL spike waveforms, their length was similar in both
586 control and ELS females (Fig. 7D). However, the FWHM of the initial negative peak of the
587 extracellular action potential was significantly longer in ELS females than in control females (control:
588 0.27 (0.15) ms, ELS: 0.37 (0.25) ms, U = 1136, p = 0.0004, Mann-Whitney test).

589 For adolescent mice, after spike sorting we obtained n = 12 single units from N = 6 control males
590 and n = 23 units from N = 9 ELS males as well as n = 52 single units from N = 14 control females
591 and n = 30 single untis from N = 14 ELS females. Our analysis revealed no significant differences in

592 either sex for any of the parameters analysed between control and ELS mice (Suppl. Fig. 7 A-D).
593 We observed a trend towards a decrease in mean firing rates in ELS males, which appears to be in
594 line with our observation in pre-juvenile males. However, due to the low number of units in controls,
595 this analysis would have to be confirmed in a larger dataset.

596 These data suggest that during pre-juvenile development, ELS leads to an overall decrease in firing
597 activity in the PL in males. Furthermore, increased population activity of inhibitory fast-spiking
598 interneurons may contribute to hypoactivity within mPFC networks after ELS in pre-juvenile males.
599 During adolescent development, ELS males showed a trend towards lower mean firing rates in PL
600 which would have to be confirmed in a larger data set.

601 In females, neither the firing rate nor the firing pattern were affected in PL by ELS, and also no
602 changes in the mAHP of the spikes were detected during either developmental time point.

603 **3.9 ELS disrupts spike-LFP synchronization both locally and between the BLAa and the**
604 **mPFC.**

605 To further characterize the effect of ELS on long-range interactions between mPFC and BLAa, we
606 sought to estimate the phase synchronization between spikes and LFP, both within and across PFC
607 and BLAa. We focussed on the superficial layers of the PL and the LFP in the 3-5 Hz low-theta band
608 in pre-juvenile mice, as impairments in coherence were observed in this frequency band and this
609 subregion of the mPFC. In the BLAa of control males, local spike firing occurred preferentially on the
610 descending phase of the theta cycle (Fig. 8Ai), with the vast majority of units (31/36, 86%) being
611 locked to the local theta rhythm. BLAa units in ELS males showed a similar preferred phase angle
612 to the local theta rhythm and a comparable locking strength as in controls, as measured by the length
613 of the mean resulting vector. The vast majority (28/29, 97%) of BLAa units in ELS males was also
614 locked to the local theta rhythm. BLAa units in control females also occurred at a similar preferred
615 phase angle to their male counterpart (Fig. 8Aii), with almost every unit being locked to the
616 descending phase of the local LFP (33/35, 94%). ELS females also showed a high proportion of
617 locked BLAa units (19/22, 86%) as well as a similar locking strength to control females, but the

preferred phase angle differed between the two groups (Watson-Williams test, $p = 0.0062$). While this difference in phase angle was consistent and statistically significant, it was only ~20° in absolute terms, meaning that the spikes were still functionally locked to a similar cycle phase in both groups.

Within the PL, both in control and ELS males, spikes occurred preferentially at the trough of the local theta cycle (Fig. 8Aiii). However, the locking strength, i.e. length of the mean resulting vector, was significantly smaller in ELS males (Mann-Whitney test, $p = 0.009$) and also the proportion of PL units locked to the local theta rhythm was much lower than in controls (control: 30/54, 56%, ELS: 7/90, 8%, Fisher´s test, $p < 0.0001$), thus indicating a desynchronization between the spiking activity and the local theta rhythm. Interestingly, none of the putative fast-spiking interneurons in PL in either treatment group showed significant locking, suggesting that locked units are mainly principal neurons. Both in control and ELS females, PL units also preferentially fired at the trough of the local theta cycle (Fig. 8Aiv). In both groups, the number of significantly locked units was low (control: 18/74, 24%, ELS: 7/49, 14%) and not different between the groups. However, as in males, there was a trend towards a decreased vector length (i.e. locking strength) in ELS females vs controls, but this did not quite reach significance (Mann-Whitney test, $p = 0.097$) probably due to the low number of locked units. Overall, while ELS caused prominent desynchronization between the firing of PL units and the local theta rhythm in males, this effect was much weaker in females, suggesting that developing prefrontal networks in males are particularly vulnerable to ELS.

When analysing long-range spike-field interactions, in control males a high percentage of BLAa units (18/22, 82%) was locked to the theta rhythm in PL, with spikes preferentially occurring on the descending phase of the PL theta cycle (Fig. 8Bi). In ELS males, a similar proportion of BLAa units was locked to the PL theta rhythm (24/25, 96%), and also the vector length was similar. However, their preferred phase angle was dramatically different (Watson-Williams test, $p < 0.0001$), displaying a ~180° inversion, with BLAa spikes being locked to the ascending phase of the PL theta cycle. In control females, also a high percentage of BLAa units (17/20, 85%) was locked to the PL theta rhythm, but in stark contrast to control males, spikes occurred preferentially on the ascending phase of the PL theta cycle (Fig. 8Bii). In ELS females, the proportion of locked BLAa units as well as the

locking strength to PL theta was similar to control females. However, as for ELS males, ELS also affected the preferred phase angle in females (Watson-Williams test, $p = 0.039$) with spikes occurring preferentially later in the cycle closer to the peak than in control females, although the difference in phase angle was not as dramatic as in males.

When analysing phaselocking of PL units to the BLAa theta rhythm, in control males the majority of PL units (20/31, 61%) was locked to the BLAa theta rhythm with spikes occurring at the descending phase of the theta cycle (Fig. 8Biii). In ELS males, very few PL units (3/55, 6%) were locked to the BLAa theta rhythm, a significantly lower proportion compared to controls (Fisher´s test, $p < 0.0001$) and none of them were putative fast-spiking interneurons. Those few units that were locked displayed also a different preferred phase angle (Watson-Williams test, $p = 0.012$) occurring earlier in the theta cycle than units in controls. In control females, similar to males, the majority of PL units was locked to the BLAa theta rhythm (13/21, 62%) with a preferred phase angle on the descending phase of the BLAa theta cycle (Fig. 8Biv). As in ELS males, also in ELS females very few PL units (4/37, 11%) were locked to the BLAa theta rhythm, significantly less than in control females (Fisher´s test, $p < 0.0001$). However, their preferred phase angle was similar as in controls. Neither in ELS males nor females the vector length was significantly different to controls, although this was difficult to assess due to the low number of locked PL units in ELS pups.

Overall, spike-LFP phaselocking analysis showed a prominent effect of ELS on the entrainment of spiking activity in the PL, predominantly in males, to both the local and the BLAa theta rhythm, resulting in a lower proportion of locked units, weaker locking strength, and a shift in the preferred phase angle. ELS females had a milder phenotype limited to long-range outcomes. Interestingly, ELS also led to a major change in the preferred phase angle of BLAa units locked to PL theta. Together with the effect of ELS on the entrainment of PL spikes, this suggests that ELS results in prominent changes in how synaptic inputs are integrated in the PL and may lead to an abnormal output from the developing PL.

4. Discussion

671 The present study shows that ELS causes major dysfunction within prefrontal-amygdala networks *in*
672 *vivo* during pre-juvenile development in a sex-dependent manner. Hence, this developmental period
673 may present a "window of opportunity" during which an abnormal developmental trajectory inflicted
674 by ELS may still be rescued. We found evidence of changes in local neuronal firing activity after
675 ELS, such as increased firing activity within BLA but decreased firing activity within mPFC. Long-
676 range functional interactions were also affected after ELS leading to exaggerated oscillatory theta
677 coupling as well as deficits in the reciprocal theta entrainment of spikes. These early impairments in
678 prefrontal-amygdala circuit function may constitute an altered developmental trajectory towards an
679 increased susceptibility to psychiatric diseases later in life.

680 **4.1 Oscillatory network activity within developing mPFC or amygdala is not affected by ELS**

681 Temporal coordination through neuronal synchrony as seen during oscillatory network activity is
682 critical for normal adult brain function [47]. Moreover, impaired oscillatory network activity has been
683 found during postnatal development in rodent models of psychiatric disorders, and may even
684 constitute an early biomarker of later disease, for review see [48]. To address if ELS also impacts
685 neuronal synchrony within developing prefrontal-amygdala networks, we performed LFP recordings
686 within pre-juvenile and adolescent prelimbic, infralimbic, and BLAa networks of control and ELS mice
687 under light urethane anaesthesia, and we analysed the PSD of frequencies spanning the 0.1-100
688 Hz range. In addition to the anaesthesia induced slow-wave activity, we found predominant activity
689 in the low-theta range (3-5 Hz) within mPFC networks at both ages. This is in line with recent reports
690 in awake mice that also describe predominant network activity in the low-theta range during resting
691 at similar ages [32]. Although we did not quantify this, our data also indicate an increase in high-theta
692 (6-12 Hz) as well as in gamma power (12-100 Hz) in the mPFC from pre-juvenile to adolescent
693 development (see Fig. 1C) similar to what has been observed in awake mice in the mPFC [32]. This
694 suggests that the gross developmental changes in prefrontal network activity are also visible and
695 preserved under anaesthesia and further justifies the focus of our analysis on the low-theta band as
696 the dominating network activity in pre-juvenile mice. However, we did not find any effect of ELS on
697 PSD neither in the mPFC nor in the BLAa. While this could be due to the technical limitation of

performing all recordings under anaesthesia, a recent preprint on the effect of ELS on low-theta power (2-5 Hz) in mPFC or amygdala of adult awake behaving mice did not find any significant changes neither during resting nor following fear conditioning (during extinction or recall) in both sexes [49]. These findings strengthen our conclusion that ELS does not impact the generation of synchronous network activity within the developing mPFC nor BLAa per se particularly in the low-theta range.

4.2 ELS leads to sex-specific prefrontal-amygdala theta-hypercoupling during pre-juvenile development

Impaired prefrontal-amygdala long-range interactions are a major disease hallmark after ELS, and are also present in subjects at risk [4, 50]. Previous studies showed impairments in prefrontal-amygdala functional connectivity obtained with fMRI both during development and in adulthood in rodent models of ELS [15, 23-25]. However, direct electrophysiological measurements of neuronal network activity in these models remain sparse [26]. We analysed coherence as a quantitative measure of oscillatory coupling within prelimbic- or infralimbic-BLAa networks. We focussed on the low-theta band (3-5 Hz), as impairments in long-range low-theta synchrony were present in our previous study in pre-juvenile ELS rat pups [26]. Moreover, theta oscillations within this frequency band are known to support long-range coordination such as fear learning and extinction, and they are also a substrate of innate anxiety [51-53]. Our findings highlight an increased coupling between the BLAa and the PL in layers II/III in the low-theta band which was specific to pre-juvenile males, while females had a milder phenotype showing only a trend towards theta hypercoupling. This is in line with previous reports also showing that early impairments in functional interactions after ELS are limited to males [23, 25, 26]. No differences in theta coupling were observed between control and ELS mice during adolescence. However, when analysing the increase in prefrontal-amygdala low-theta coherence from pre-juvenile development to adolescence, we found that this increase was significantly lower in both ELS males and females, which may indicate a precocious development of coupling strength after ELS. Previous studies showed a decrease in functional interactions within prefrontal-amygdala networks after ELS in pre-juvenile rats [23, 25, 26] using either MS or LBN as a stress model. Differences between species,

725 in the stress paradigm, and particularly in the timing of stress exposure may underlie the different
726 outcomes in the valence of the effect between those of the previous and our study. However, in line
727 with those previous studies we also found that the effect of ELS on developing prefrontal-amygdala
728 networks is not linear, i.e. it does not simply increase over time, but rather it is confined to certain
729 developmental windows, often during juvenile development, which appear to be more susceptible to
730 stress[6, 25, 40]. Accordingly, early theta-hypercoupling during pre-juvenile development may either
731 correspond to the previously described accelerated development of prefrontal amygdala circuits or
732 may constitute an impairment confined to pre-juvenile development which seems to be particularly
733 vulnerable to ELS. Further studies are necessary to corroborate this finding and its meaning.
734 Interestingly, similar cumulative ELS (LBN+MS) in mice also resulted in increased resting state
735 functional connectivity [15] as well as anatomical hyperconnectivity [24] during adulthood in males only,
736 which strongly correlated with an anxiety phenotype [15]. Behavioural characterization of our LBN+MS
737 ELS model during adulthood revealed increased anxiety-like behaviours in ELS males and strong
738 deficits in classical fear conditioning in both ELS males and females[27]. Future studies are needed to
739 confirm if hypercoupling within prefrontal-amygdala networks also emerges during adulthood in our
740 ELS model and contributes or underlies an anxiety phenotype. **4.3 ELS leads to chronic increase
741 in firing activity of a subpopulation of putative (non-GABAergic) principal neurons in the
742 BLAa during pre-juvenile development and to a more widespread increase in mean firing
743 rates during adolescence**

744 Analysis of *in vivo* spike firing activity as well as immunohistochemistry against ΔFosB in pre-juvenile
745 BLAa suggest that ELS leads to an increase in firing activity of a subpopulation of BLAa neurons
746 already during brain development. Increased activity of amygdala neurons after ELS has been
747 previously described as an increase in the number of cFos positive neurons in response to a stressful
748 stimulus [16, 17]. Furthermore, amygdala hyper-reactivity is one of the most consistent findings after
749 ELS in humans [4]. Here we extend these findings to ELS models, and we show for the first time that
750 ELS also leads to higher baseline firing rates in a subpopulation of BLAa neurons *in vivo* in either
751 sex. The shorter valley-to-peak time of the spike waveforms in ELS males vs controls (corresponding

752 to the medium afterhyperpolarization, mAHP) is a further indicator of increased excitability of BLAa
753 neurons after ELS. Chronic stress during either adolescence or adulthood has previously been
754 shown to lead to a decrease in the amplitude of the mAHP, as well as to an increase in the intrinsic
755 excitability of BLA pyramidal neurons in *in vitro* brain slice recordings in adult rats or mice [20, 54]. These
756 changes were due to the loss of currents from small-conductance calcium-activated potassium
757 channels containing subunit 2 (SK_2), e.g. by reduced expression after ELS [20, 54]. Furthermore, altered
758 excitatory neuropeptide release may also contribute to the reduced mAHP and potentially increased
759 neuronal excitability in BLAa after ELS. For example, corticotropin-releasing hormone (CRH) is
760 expressed in a significant population of BLA neurons[55] and has been shown to positively modulate
761 neuronal excitability through effects on potassium channels and is also known to lead to a decrease
762 in AHP decay time[56].

763 Further experiments are needed to reveal if downregulation of SK_2 channels and or altered CRH
764 release after ELS in male pre-juvenile BLAa also underlies the change in length of the mAHP in our
765 ELS model, which may promote increased baseline firing rates at least in a subpopulation of BLAa
766 neurons. Of note, we did not find any changes in the valley-to-peak time of BLAa spikes in female
767 pre-juvenile pups, suggesting that the increase in baseline firing of a subpopulation of BLAa units in
768 females may have a different underlying mechanism than in males. Our analysis of BLAa neuronal
769 activity during adolescence revealed an even stronger and more widespread increase in mean firing
770 rates in ELS males as well as impaired firing patterns compared to controls, suggesting that the
771 phenotype further increased from pre-juvenile to adolescent development. The data in adolescent
772 females point to a similar phenotype as in males, but would have to be confirmed in a larger dataset.
773 The decrease in BLAa spike FWHM in both ELS males and females suggests either altered
774 expression of ion channels such a sodium or calcium channels after ELS or may result from the
775 chronic increase in activity of these neurons. Most likely these neurons with higher baseline firing
776 activity mostly comprise BLAa principal neurons, as we did not find any indication from correlation
777 or clustering analysis for increased activation of FSIs. Interestingly, the decrease in valley-to-peak
778 time corresponding to mAHP did no longer persist in ELS males during adolescence, but was present

779 in ELS females instead, suggesting increased excitability of BLAa neurons in adolescent females
780 and combined with the decreased half-width of the spike and overall shorter spike duration.

781 In line with the effect of ELS on pre-juvenile spike firing in BLAa, our immunohistochemistry data
782 showing an increase in ΔFosB$^+$ neurons in the BLAa after ELS in both sexes provides further
783 evidence that ELS leads to a persistent increase in neuronal firing activity of a subpopulation of
784 neurons within pre-juvenile BLAa. The Δ splice variant of the immediate early gene FosB is a suitable
785 marker for the effect of chronic stress on neuronal activity [43] and has previously been shown to also
786 respond to chronic stress within the developing amygdala in rats [57]. Due to the unavailability of
787 commercial antibodies against ΔFosB, double staining against PanFosB and FosB to identify
788 neurons expressing ΔFosB has been precedently established as an alternative method [58] and has
789 also worked well in our study. Interestingly, while in males the increase in ΔFosB$^+$ neurons was
790 independent of age and already present right after the end of the chronic stress period, in females it
791 only emerged at P18, which may point to a different underlying mechanism for the increase in
792 neuronal activity than in males. Future experiments are needed to reveal the identity of the activated
793 neurons, and whether they share a specific projection target or they receive a distinct set of inputs.
794 Our triple immunohistochemical staining against ΔFosB and GAD67 already revealed that ΔFosB$^+$
795 neurons were GAD67 immunonegative in pre-juvenile males, while in pre-juvenile females some
796 double positive neurons were encountered. Hence, the vast majority of those chronically activated
797 neurons in the pre-juvenile BLAa do not seem to be GABAergic interneurons. It has previously been
798 shown that chronic stress in adulthood leads to the activation of neurons that project to the ventral
799 hippocampus (vHipp), which is associated with a selective decrease in SK_2 channel currents as well
800 as an increased intrinsic excitability in these cells [54]. Moreover, overexpression of SK_2 channels in
801 vHipp-projecting BLA neurons rescued the anxiety phenotype after ELS. Future research will show
802 whether similar target specificity also applies to developing BLA neurons activated by ELS.

803 **4.4 ELS leads to a decrease in firing rates *in vivo* in the pre-juvenile PL in males**

804 In contrast to the BLAa, where ELS resulted in an increased activity of a subpopulation of neurons,
805 its effect on baseline firing activity within layer II/III of the pre-juvenile PL was broadly inhibitory. In
806 males, mean baseline firing rates of PL units were decreased in ELS pups compared to controls.
807 Our results are in line with previous data claiming that ELS leads to inhibition of the mPFC. It has
808 been shown that ELS leads to a decrease in synaptic spine density on pyramidal cells within both
809 the superficial and the deep layers of the adult PL, which is associated with decreased glutamatergic
810 transmission in the PL after ELS [59]. Accordingly, chemogenetic activation of PL pyramidal neurons
811 in ELS pups rescued deficits in working memory performance. Furthermore, in line with the
812 hypothesis that ELS leads to an accelerated development, the GABA switch from excitatory to
813 inhibitory and also the downregulation of the excitation/inhibition balance happens earlier after ELS,
814 leading to an attenuated excitatory tone within the developing mPFC [60, 61]. Finally, chemogenetic
815 postnatal inhibition of the mPFC between P2-17 resulted in similar cognitive deficits in adulthood as
816 those observed following ELS, and chemogenetic activation of the mPFC during ELS was able to
817 prevent cognitive deficits in adulthood [62]. Our data contribute to this literature and show, for the first
818 time, that ELS also results in decreased firing rates in the mPFC *in vivo* already during pre-juvenile
819 development. This decrease in firing rates may hamper the ability of the mPFC to control subcortical
820 networks such as the BLAa, which may further result in increased neuronal activity therein, and may
821 promote disease symptoms after ELS. Interestingly, we did not find an effect of ELS on PL mean
822 firing rates in pre-juvenile females, suggesting a milder phenotype in females. However, the increase
823 in half-width after ELS also suggests that ELS may alter the expression or function of, e.g. K^+-
824 channels on PL pyramidal neurons, thus affecting the repolarization phase of the action potential.
825 Future studies are necessary to further explore the functional meaning of such changes for PL
826 network activity in pre-juvenile females. Interestingly, none of the changes in spike firing observed
827 during pre-juvenile development persisted during adolescence, suggesting that pre-juvenile PL is
828 particularly vulnerale to ELS. However, a trend towards decreased firing rates in PL of adolescent
829 ELS males compared to controls may point to an inhibitory effect of ELS on PL network activity also
830 during adolescence. However, this would have to be confirmed in a larger dataset.

831 **4.5 ELS differentially affects spike-LFP synchrony in males and females**

832 The Amy and the PFC are tightly interconnected in a bidirectional circuit, with the Amy sending
833 salience information to the PFC, and in turn receiving top-down regulatory inputs [63]. While our
834 coherence analysis revealed abnormal hypercoupling within prelimbic-BLAa networks after ELS in
835 pre-juvenile males, this analysis did not provide any information regarding the effect of ELS on
836 directionality within this network, i.e. whether interactions from Amy→mPFC or from mPFC→Amy
837 were affected. Hence, we analysed the phaselocking of spikes in the PL and in the BLAa to either
838 the local low-theta rhythm or long-range to the low-theta rhythm in the BLAa or in the PL,
839 respectively. Phase synchronization supports functional communication between distant areas
840 through coordinated spiking activity at specific oscillatory phases [64-66]. While the entrainment of BLAa
841 spikes to the local theta rhythm was not affected by ELS, the entrainment of PL spikes to the local
842 theta rhythm was impaired after ELS in pre-juvenile males, resulting in much lower locking strength
843 as well as a much smaller proportion of locked units. Moreover, the ability of the BLAa to entrain PL
844 spikes to the BLAa theta rhythm was also hampered after ELS particularly in males, resulting in only
845 a minority of units displaying significant locking, as well as a change in the phase angle. The dramatic
846 decrease in the ability of both the local theta rhythm and the theta rhythm in the BLAa to entrain PL
847 firing after ELS in males strongly suggest that ELS leads to major changes in the integration of
848 synaptic inputs in the PL likely resulting in a desynchronized output of spike firing. This may be due
849 to changes in the anatomical connectivity as hyperconnectivity between mPFC and amygdala has
850 been found in a similar ELS model in pre-juvenile [26] or adult males [24]. Furthermore, a decrease in
851 synaptic spine density on pyramidal cells within the PL that has been shown to be associated with
852 diminished glutamatergic transmission and a decreased expression of GluR1 and NR1 subunits of
853 AMPA or NMDA receptors after ELS [59] may also be a contributing factor. Finally, changes in the
854 excitation/inhibition balance due to the impact of ELS on the development of e.g. PV^+ interneurons
855 [67] may also affect the integration of synaptic inputs, leading to poor entrainment of PL units.
856 Moreover, while PL theta was still able to entrain the firing of BLAa units after ELS in both sexes (i.e.
857 locking strength and percentage of locked units were similar to controls), the phase angle (i.e. the

858 timing within the theta cycle) had dramatically shifted after ELS, particularly in males. This further
859 supports altered synaptic integration within these networks after ELS. Since the precise timing of
860 BLA spikes to PFC theta is critical for information transfer from PFC to BLA (i.e. top-down control)
861 to signal safety during both learned and innate anxiety [53], dramatic phase-shifts in locking of BLA
862 spikes to PL theta may also interfere with the ability of PFC to dynamically control activity within BLA
863 networks as well as the anxiety response. Hence, our results suggest that ELS affects interactions
864 in both directions from BLAa to PL as well as top-down from PL to BLAa in pre-juvenile males. In
865 females, the effect of ELS on theta entrainment of spikes within or across PL or BLAa where much
866 milder than in males, in line with an only mild effect of ELS on theta coherence in females. This is in
867 accordance with previous reports that females are less susceptible to ELS than males in rodent
868 models [19, 24, 26]. Further studies are needed to understand whether abnormal functional interactions
869 are only transient or are also present in adulthood, and if they underlie increased anxiety or abnormal
870 fear learning in this model.

871 **4.6 Effect of urethane anaesthesia on neuronal network activity**

872 *In vivo* electrophysiological recordings in young mice bare their own challenges. Head-implants for
873 freely-moving recordings are usually too heavy and may interfere with nursing. Head-fixed
874 recordings lead to a strong acute restrained-stress response which is known to strongly activity BLA
875 in adult rodents and may overlay any chronic changes in activity due to ELS. Therefore, we opted to
876 perform *in vivo* electrophysiological recordings in developing mice under anaesthesia. It has been
877 previously shown that brain activity under urethane anaesthesia closely resembles that under natural
878 sleep. For instance, cyclical alternations of brain state during sleep and the alternations induced by
879 urethane are remarkably similar[37]. This suggests that such a high similarity likely reflects shared
880 physiological mechanisms between sleep and urethane-induced anaesthesia, rendering urethane
881 as an anaesthetic ideally suitable for studies examining cyclical brain rhythms. This also has been
882 confirmed when investigating the effect of urethane on network activity during brain development[68].
883 Moreover, urethane only minimally alters neuronal firing patterns compared to other anaesthetics[69]
884 The cortical neuronal network activity under anaesthesia we observed was dominated by low-theta

885 oscillations (3-5 Hz), similar to cortical network activity recorded in head-fixed awake mice at similar
886 ages[32]. Therefore, we believe that the neuronal network activity we recorded under urethane
887 anaesthesia shares similar physiological mechanism with network activity in awake rodents at similar
888 ages during natural sleep and to some extent under quiet resting conditions. However, how our data
889 compares to network activity in awake freely moving animals at similar ages and how ELS may affect
890 neuronal network activity during active behaviours such as exploration, decision making or fear
891 learning has to be investigated in future studies.

892 **4.7 Sex differences in the effect of ELS on developing prefrontal-amygdala network activity**

893 It has been widely demonstrated, that ELS seems to have sex-specific effects in rodent models but
894 also in exposed humans[24,70]. Typically, either males show a stronger phenotype than females or ELS
895 seems to affect different behavioural traits. For example, it has been shown that ELS specifically
896 promotes depressive-like behaviours in female rodents [14]. In line with these previous findings, our
897 data also shows stronger effects of ELS in males than females. We observed an increased in
898 coherence in prelimbic-amygdala networks only in pre-juvenile males but not females and also the
899 effect of ELS on spike firing in either PFC or BLAa seem stronger in males than in females. Similarly,
900 theta entrainment of spikes within prefrontal-amygdala networks was also more strongly affected in
901 males than in females. Several complementary mechanisms may contribute to the enhanced male
902 vulnerability we observed. Males show higher baseline rates of neuronal apoptosis during
903 development[71], which could create greater susceptibility to stress-induced cellular damage during
904 critical developmental windows. Additionally, sex differences in stress hormone receptor expression
905 and sensitivity may amplify the impact of developmental stress exposure in males compared to
906 females. The timing of our stress protocol (P4-P14) corresponds to a critical time window for
907 development, when sex differences in neural maturation are emerging, potentially resulting in
908 different outcomes despite the stressor being equal. Our electrophysiological findings may reflect
909 this differential developmental trajectory, with males showing more pronounced disruptions in
910 neuronal functional properties following ELS. Future studies are needed to further our understanding
911 on the underlying mechanism leading to distinct outcomes of ELS in males versus females.

912

913 **5. Integrative framework and conclusions**

914 Here we show that ELS leads to theta hypercoupling within prefrontal-amygdala networks during
915 pre-juvenile development only, particularly in male pups (Fig. 9). This early hypercoupling is either
916 the result of precocious development and may be independent of any deficits in directed interactions,
917 or may constitute a developmental impairment limited to pre-juvenile development as particularly
918 vulnerable to ELS. Alternatively, it may be driven by a third region such as the ventral hippocampus,
919 which has strong anatomical connectivity with both the mPFC and the BLA. The emerging theta
920 hypercoupling may constitute a compensatory mechanism to an awry reciprocal entrainment within
921 developing prefrontal-amygdala networks. Furthermore, in both males and females, ELS caused a
922 chronic increase in neuronal spiking activity of a subpopulation of neurons in pre-juvenile BLAa,
923 which were non-GABAergic and hence most likely principal neurons. Moreover, in ELS males this
924 phenotype further increased during adolescence, leading to a prominent increase in mean firing
925 rates in a wider population of BLAa neurons. In contrast, in the mPFC, ELS resulted in a net decrease
926 in neuronal firing activity in male pre-juvenile pups. We also showed that directed interactions by
927 theta entrainment of spikes across prelimbic-amygdala networks are also impacted by ELS in pre-
928 juvenile males, leading to weak locking of PL units to both the local and BLA theta rhythms. Overall,
929 our data suggests that ELS has profound effects on the functional development of mPFC networks
930 particularly during pre-juvenile development, leading to a dampened firing activity, i.e. output which
931 is not synchronized and hard to entrain by subcortical networks such as the BLA, but also affects
932 the timing and integration of synaptic inputs within the mPFC. These impairments may increase
933 susceptibility to disease leading to aberrant development of emotional behaviours or cognitive
934 abilities after ELS. Moreover, early impairments in functional coupling as well as directed interactions
935 may impact fear and safety learning. Theta hypercoupling may compromise the ability of the network
936 to express fine-tuned increases and decreases in prefrontal-amygdala theta synchrony, which are
937 associated with fear acquisition and extinction learning [53, 65]. Since safety is signalled by the mPFC
938 entraining BLA firing via oscillatory theta band activity [53], ELS-evoked major phase shifts in theta

939 entrainment may be disruptive. This could result in fear generalization, as animals that generalize
940 fear show high theta power and synchrony to both aversive and non-aversive cues and lack the
941 prefrontal theta entrainment of BLA networks [53]. However, also an opposite effect on fear and anxiety
942 behaviours may be possible. Since we observed major deficits in BLA theta entrainment of PL
943 spikes, i.e. disruption of bottom-up communication critical to signal potential threats in the
944 environment, juvenile animals may also become less anxious after ELS.

945 We identified major impairments in prefrontal-amygdala network function following ELS already
946 during pre-juvenile development. Hence, this developmental period may open a window of
947 opportunity during which targeted interventions could prevent the emergence of a disease phenotype
948 during adulthood. Future studies are needed to understand if these impairments within pre-juvenile
949 development lead to persistent changes in the developmental trajectory of prefrontal-amygdala
950 network function, if and how they contribute to a behavioural phenotype, and whether interventions
951 during this developmental window can prevent future disease symptoms.

952 **Acknowledgments**

953 We thank Assel Kalmenova and Nicolas Vetter for technical help. This study was financially
954 supported by the Research Council of Finland (project grant (decision no 333341) to H.H.

955 **Author contributions**

956 A.D. and F.V. performed the *in vivo* electrophysiological recordings, F.V. analysed LFP data, A.D.
957 performed spike sorting and analysed single unit activity, A.D. performed all immunohistochemistry
958 and image analysis, H.H. provided resources for the experimental work and supervised the project.
959 H.H. conceptualized and coordinated the project. The manuscript was written by H.H. with significant
960 contributions from all authors.

961 **Conflict of interest statement:** The authors declare no conflict of interest.

962 **References**

963 1. Carr CP, Martins CM, Stingel AM, Lemgruber VB, Juruena MF. The role of early life stress
964 in adult psychiatric disorders: a systematic review according to childhood trauma subtypes.
965 *The Journal of nervous and mental disease* 2013; **201**(12)**:** 1007-1020.

966
967 2. Green JG, McLaughlin KA, Berglund PA, Gruber MJ, Sampson NA, Zaslavsky AM *et al.*
968 Childhood adversities and adult psychiatric disorders in the national comorbidity survey
969 replication I: associations with first onset of DSM-IV disorders. *Arch Gen Psychiatry* 2010;
970 **67**(2)**:** 113-123.

971
972 3. Weber K, Rockstroh B, Borgelt J, Awiszus B, Popov T, Hoffmann K *et al.* Stress load during
973 childhood affects psychopathology in psychiatric patients. *BMC psychiatry* 2008; **8:** 63.

974
975 4. VanTieghem MR, Tottenham N. Neurobiological Programming of Early Life Stress:
976 Functional Development of Amygdala-Prefrontal Circuitry and Vulnerability for Stress-
977 Related Psychopathology. *Current topics in behavioral neurosciences* 2018; **38:** 117-136.

978
979 5. Guadagno A, Belliveau C, Mechawar N, Walker CD. Effects of Early Life Stress on the
980 Developing Basolateral Amygdala-Prefrontal Cortex Circuit: The Emerging Role of Local
981 Inhibition and Perineuronal Nets. *Frontiers in human neuroscience* 2021; **15:** 669120.

982
983 6. Callaghan BL, Tottenham N. The Stress Acceleration Hypothesis: Effects of early-life
984 adversity on emotion circuits and behavior. *Curr Opin Behav Sci* 2016; **7:** 76-81.

985
986 7. Rice CJ, Sandman CA, Lenjavi MR, Baram TZ. A novel mouse model for acute and long-
987 lasting consequences of early life stress. *Endocrinology* 2008; **149**(10)**:** 4892-4900.

988
989 8. Bolton JL, Short AK, Simeone KA, Daglian J, Baram TZ. Programming of Stress-Sensitive
990 Neurons and Circuits by Early-Life Experiences. *Front Behav Neurosci* 2019; **13:** 30.

991
992 9. Gallo M, Shleifer DG, Godoy LD, Ofray D, Olaniyan A, Campbell T *et al.* Limited Bedding
993 and Nesting Induces Maternal Behavior Resembling Both Hypervigilance and Abuse. *Front*
994 *Behav Neurosci* 2019; **13:** 167.

995
996 10. Naninck EF, Hoeijmakers L, Kakava-Georgiadou N, Meesters A, Lazic SE, Lucassen PJ *et*
997 *al.* Chronic early life stress alters developmental and adult neurogenesis and impairs
998 cognitive function in mice. *Hippocampus* 2015; **25**(3)**:** 309-328.

999
1000 11. Bolton JL, Schulmann A, Garcia-Curran MM, Regev L, Chen Y, Kamei N *et al.* Unexpected
1001 Transcriptional Programs Contribute to Hippocampal Memory Deficits and Neuronal
1002 Stunting after Early-Life Adversity. *Cell Rep* 2020; **33**(11)**:** 108511.

1003
1004 12. Manzano Nieves G, Bravo M, Baskoylu S, Bath KG. Early life adversity decreases pre-
1005 adolescent fear expression by accelerating amygdala PV cell development. *Elife* 2020; **9**.

1006
1007 13. Sanguino-Gómez J, Huijgens S, den Hartog M, Schenk IJM, Kluck W, Versluis TD *et al.*
1008 Neural correlates of learning and memory are altered by early-life stress. *Neurobiol Learn*
1009 *Mem* 2024; **213:** 107952.

14. Goodwill HL, Manzano-Nieves G, Gallo M, Lee HI, Oyerinde E, Serre T *et al.* Early life stress leads to sex differences in development of depressive-like outcomes in a mouse model. *Neuropsychopharmacology : official publication of the American College of Neuropsychopharmacology* 2018.

15. Johnson FK, Delpech JC, Thompson GJ, Wei L, Hao J, Herman P *et al.* Amygdala hyper-connectivity in a mouse model of unpredictable early life stress. *Transl Psychiatry* 2018; **8**(1)**:** 49.

17. Malter Cohen M, Jing D, Yang RR, Tottenham N, Lee FS, Casey BJ. Early-life stress has persistent effects on amygdala function and development in mice and humans. *Proc Natl Acad Sci U S A* 2013; **110**(45)**:** 18274-18278.

18. Guadagno A, Verlezza S, Long H, Wong TP, Walker CD. It Is All in the Right Amygdala: Increased Synaptic Plasticity and Perineuronal Nets in Male, But Not Female, Juvenile Rat Pups after Exposure to Early-Life Stress. *The Journal of neuroscience : the official journal of the Society for Neuroscience* 2020; **40**(43)**:** 8276-8291.

19. Guadagno A, Wong TP, Walker CD. Morphological and functional changes in the preweaning basolateral amygdala induced by early chronic stress associate with anxiety and fear behavior in adult male, but not female rats. *Prog Neuro-Psychoph* 2018; **81:** 25-37.

20. Rau AR, Chappell AM, Butler TR, Ariwodola OJ, Weiner JL. Increased Basolateral Amygdala Pyramidal Cell Excitability May Contribute to the Anxiogenic Phenotype Induced by Chronic Early-Life Stress. *The Journal of neuroscience : the official journal of the Society for Neuroscience* 2015; **35**(26)**:** 9730-9740.

21. Yan CG, Rincon-Cortes M, Raineki C, Sarro E, Colcombe S, Guilfoyle DN *et al.* Aberrant development of intrinsic brain activity in a rat model of caregiver maltreatment of offspring. *Transl Psychiatry* 2017; **7**(1)**:** e1005.

22. Bolton JL, Molet J, Regev L, Chen Y, Rismanchi N, Haddad E *et al.* Anhedonia Following Early-Life Adversity Involves Aberrant Interaction of Reward and Anxiety Circuits and Is Reversed by Partial Silencing of Amygdala Corticotropin-Releasing Hormone Gene. *Biol Psychiatry* 2018; **83**(2)**:** 137-147.

23. Guadagno A, Kang MS, Devenyi GA, Mathieu AP, Rosa-Neto P, Chakravarty M *et al.* Reduced resting-state functional connectivity of the basolateral amygdala to the medial prefrontal cortex in preweaning rats exposed to chronic early-life stress. *Brain Struct Funct* 2018; **223**(8)**:** 3711-3729.

24. White JD, Arefin TM, Pugliese A, Lee CH, Gassen J, Zhang J *et al.* Early life stress causes sex-specific changes in adult fronto-limbic connectivity that differentially drive learning. *Elife* 2020; **9**.

1058 25. Honeycutt JA, Demaestri C, Peterzell S, Silveri MM, Cai X, Kulkarni P *et al.* Altered
1059 corticolimbic connectivity reveals sex-specific adolescent outcomes in a rat model of early
1060 life adversity. *Elife* 2020; **9**.

1061
1062 26. Haikonen J, Englund J, Amarilla SP, Kharybina Z, Shintyapina A, Kegler K *et al.* Aberrant
1063 cortical projections to amygdala GABAergic neurons contribute to developmental circuit
1064 dysfunction following early life stress. *iScience* 2023; **26**(1)**:** 105724.

1065 27. Shteinikov V, Rhee JK, Ojanen S, Kunnari AJ, Haikonene J, Picard M, et al. Aberrant
1066 development of glutamatergic inputs to PV and SOM interneurons shape amygdala
1067 excitability and oscillatory dynamics after early life stress. bioRxiv. 2025 Jan
1068 1;2025.08.30.673226.

1069
1070 28. Bath KG, Manzano-Nieves G, Goodwill H. Early life stress accelerates behavioral and
1071 neural maturation of the hippocampus in male mice. *Horm Behav* 2016; **82:** 64-71.

1072
1073 29. Arruda-Carvalho M, Wu WC, Cummings KA, Clem RL. Optogenetic Examination of
1074 Prefrontal-Amygdala Synaptic Development. *The Journal of neuroscience : the official*
1075 *journal of the Society for Neuroscience* 2017; **37**(11)**:** 2976-2985.

1076
1077 30. Bouwmeester H, Smits K, Van Ree JM. Neonatal development of projections to the
1078 basolateral amygdala from prefrontal and thalamic structures in rat. *J Comp Neurol* 2002;
1079 **450**(3)**:** 241-255.

1080
1081 31. Bitzenhofer SH, Popplau JA, Chini M, Marquardt A, Hanganu-Opatz IL. A transient
1082 developmental increase in prefrontal activity alters network maturation and causes
1083 cognitive dysfunction in adult mice. *Neuron* 2021; **109**(8)**:** 1350-1364 e1356.

1084
1085 32. Popplau JA, Schwarze T, Dorofeikova M, Pochinok I, Gunther A, Marquardt A *et al.*
1086 Reorganization of adolescent prefrontal cortex circuitry is required for mouse cognitive
1087 maturation. *Neuron* 2024; **112**(3)**:** 421-440 e427.

1088
1089 33. Rutishauser U, Ross IB, Mamelak AN, Schuman EM. Human memory strength is predicted
1090 by theta-frequency phase-locking of single neurons. *Nature* 2010; **464**(7290)**:** 903-907.

1091
1092 34. Berens P. CircStat: A MATLAB Toolbox for Circular Statistics. *J Stat Softw* 2009; **31**(10)**:** 1-
1093 21.

1094
1095 35. Riga D, Kramvis I, Koskinen MK, van Bokhoven P, van der Harst JE, Heistek TS *et al.*
1096 Hippocampal extracellular matrix alterations contribute to cognitive impairment associated
1097 with a chronic depressive-like state in rats. *Sci Transl Med* 2017; **9**(421).

1098
1099 36. Mroue-Ruiz FH, Garvin M, Ouellette L, Sequeira MK, Lichtenstein H, Kar U *et al.* Limited
1100 Bedding and Nesting as a Model for Early-Life Adversity in Mice. *Journal of visualized*
1101 *experiments : JoVE* 2024; (209).

1102

1103 37. Clement EA, Richard A, Thwaites M, Ailon J, Peters S, Dickson CT. Cyclic and sleep-like
1104 spontaneous alternations of brain state under urethane anaesthesia. *PLoS One* 2008; **3**(4)**:**
1105 e2004.

1106
1107 38. Pagliardini S, Gosgnach S, Dickson CT. Spontaneous sleep-like brain state alternations
1108 and breathing characteristics in urethane anesthetized mice. *PLoS One* 2013; **8**(7)**:**
1109 e70411.

1110
1111 39. Whitten TA, Martz LJ, Guico A, Gervais N, Dickson CT. Heat synch: inter- and
1112 independence of body-temperature fluctuations and brain-state alternations in urethane-
1113 anesthetized rats. *J Neurophysiol* 2009; **102**(3)**:** 1647-1656.

1114
1115 40. Gee DG, Gabard-Durnam LJ, Flannery J, Goff B, Humphreys KL, Telzer EH *et al.* Early
1116 developmental emergence of human amygdala-prefrontal connectivity after maternal
1117 deprivation. *Proc Natl Acad Sci U S A* 2013; **110**(39)**:** 15638-15643.

1118
1119 41. Fareri DS, Tottenham N. Effects of early life stress on amygdala and striatal development.
1120 *Developmental cognitive neuroscience* 2016; **19:** 233-247.

1121
1122 42. Dwivedi D, Bhalla US. Physiology and Therapeutic Potential of SK, H, and M Medium
1123 AfterHyperPolarization Ion Channels. *Front Mol Neurosci* 2021; **14:** 658435.

1124
1125 43. Nestler EJ. ΔFosB: a transcriptional regulator of stress and antidepressant responses. *Eur*
1126 *J Pharmacol* 2015; **753:** 66-72.

1127
1128 44. Englund J, Haikonen J, Shteinikov V, Amarilla SP, Atanasova T, Shintyapina A *et al.*
1129 Downregulation of kainate receptors regulating GABAergic transmission in amygdala after
1130 early life stress is associated with anxiety-like behavior in rodents. *Transl Psychiatry* 2021;
1131 **11**(1)**:** 538.

1132
1133 45. Hintiryan H, Bowman I, Johnson DL, Korobkova L, Zhu M, Khanjani N *et al.* Connectivity
1134 characterization of the mouse basolateral amygdalar complex. *Nat Commun* 2021; **12**(1)**:**
1135 2859.

1136
1137 46. Manoocheri K, Carter AG. Rostral and caudal basolateral amygdala engage distinct circuits
1138 in the prelimbic and infralimbic prefrontal cortex. *Elife* 2022; **11**.

1139
1140 47. Uhlhaas PJ, Singer W. Neural Synchrony in Brain Disorders: Relevance for Cognitive
1141 Dysfunctions and Pathophysiology. *Neuron* 2006; **52**(1)**:** 155-168.

1142
1143 48. Günther A, Hanganu-Opatz IL. Neuronal oscillations: early biomarkers of psychiatric
1144 disease? *Front Behav Neurosci* 2022; **16:** 1038981.

1145
1146 49. Scarpa G, Antonoudiou P, Weiss G, Stone B, Maguire JL. Sex-dependent effects of early
1147 life stress on network and behavioral states. *bioRxiv 2024 May 10:2024.05.10.593547.*

1148

1149 50. Gerin MI, Viding E, Herringa RJ, Russell JD, McCrory EJ. A systematic review of childhood
1150 maltreatment and resting state functional connectivity. *Developmental cognitive*
1151 *neuroscience* 2023; **64:** 101322.

1152
1153 51. Karalis N, Dejean C, Chaudun F, Khoder S, Rozeske RR, Wurtz H *et al.* 4-Hz oscillations
1154 synchronize prefrontal-amygdala circuits during fear behavior. *Nat Neurosci* 2016; **19**(4)**:**
1155 605-612.

1156
1157 52. Taub AH, Perets R, Kahana E, Paz R. Oscillations Synchronize Amygdala-to-Prefrontal
1158 Primate Circuits during Aversive Learning. *Neuron* 2018; **97**(2)**:** 291-298.e293.

1159
1160 53. Likhtik E, Stujenske JM, Topiwala MA, Harris AZ, Gordon JA. Prefrontal entrainment of
1161 amygdala activity signals safety in learned fear and innate anxiety. *Nat Neurosci* 2014;
1162 **17**(1)**:** 106-113.

1163
1164
1165 54. Zhang WH, Liu WZ, He Y, You WJ, Zhang JY, Xu H *et al.* Chronic Stress Causes
1166 Projection-Specific Adaptation of Amygdala Neurons via Small-Conductance Calcium-
1167 Activated Potassium Channel Downregulation. *Biol Psychiatry* 2019; **85**(10)**:** 812-828.

1168 55. Itoga CA, Chen Y, Fateri C, Tatiana P, Lai JC, Delgado J, et al. New viral-genetic mapping
1169 uncovers an enrichment of corticotropin-releasing hormone-expressing neuronal inputs to
1170 the nucleus accumbens from stress-related brain regions. Journal of comparative
1171 neurology. 2019 Oct 15;527(15):2474–87.

1172
1173

1174 56. Gunn BG, Cox CD, Chen Y, M. Frotscher, Gall CM, Baram TZ, et al. The Endogenous
1175 Stress Hormone CRH Modulates Excitatory Transmission and Network Physiology in
1176 Hippocampus. Cerebral Cortex. 2017 Apr 28;27(8):4182–98.

1177 57. Kovács L, Füredi N, Ujvári B, Golgol A, Gaszner B. Age-Dependent FOSB/ΔFOSB
1178 Response to Acute and Chronic Stress in the Extended Amygdala, Hypothalamic
1179 Paraventricular, Habenular, Centrally-Projecting Edinger-Westphal, and Dorsal Raphe
1180 Nuclei in Male Rats. *Front Aging Neurosci* 2022; **14:** 862098.

1181

1182
1183 58. Lamothe-Molina PJ, Franzelin A, Beck L, Li D, Auksutat L, Fieblinger T *et al.* DeltaFosB
1184 accumulation in hippocampal granule cells drives cFos pattern separation during spatial
1185 learning. *Nat Commun* 2022; **13**(1)**:** 6376.

1186
1187 59. Xu L, Liu Y, Long J, He X, Xie F, Yin Q *et al.* Loss of spines in the prelimbic cortex is
1188 detrimental to working memory in mice with early-life adversity. *Mol Psychiatr* 2023; **28**(8)**:**
1189 3444-3458.

1190
1191 60. Karst H, Droogers WJ, van der Weerd N, Damsteegt R, van Kronenburg N, Sarabdjitsingh
1192 RA *et al.* Acceleration of GABA-switch after early life stress changes mouse prefrontal
1193 glutamatergic transmission. *Neuropharmacology* 2023; **234:** 109543.

1194

61. Karst H, Sarabdjitsingh RA, van der Weerd N, Feenstra E, Damsteegt R, Joëls M. Age-dependent shift in spontaneous excitation-inhibition balance of infralimbic prefrontal layer II/III neurons is accelerated by early life stress, independent of forebrain mineralocorticoid receptor expression. *Neuropharmacology* 2020; **180:** 108294.

62. Menezes EC, Geiger H, Abreu FF, Rachmany L, Wilson DA, Alldred MJ *et al.* Early-life prefrontal cortex inhibition and early-life stress lead to long-lasting behavioral, transcriptional, and physiological impairments. *Mol Psychiatr* 2024; **29**(8)**:** 2359-2371.

63. Davis M, Whalen PJ. The amygdala: vigilance and emotion. *Mol Psychiatry* 2001; **6**(1)**:** 13-34.

64. Fell J, Axmacher N. The role of phase synchronization in memory processes. *Nat Rev Neurosci* 2011; **12**(2)**:** 105-118.

65. Likhtik E, Paz R. Amygdala-prefrontal interactions in (mal)adaptive learning. *Trends Neurosci* 2015; **38**(3)**:** 158-166.

66. Palva JM, Palva S. Functional integration across oscillation frequencies by cross-frequency phase synchronization. *Eur J Neurosci* 2018; **48**(7)**:** 2399-2406.

67. Ellis SN, Honeycutt JA. Sex Differences in Affective Dysfunction and Alterations in Parvalbumin in Rodent Models of Early Life Adversity. *Front Behav Neurosci* 2021; **15:** 741454.

68. Chini M, Gretenkord S, Kostka JK, Pöpplau JA, Cornelissen L, Berde CB, et al. Neural Correlates of Anesthesia in Newborn Mice and Humans. Frontiers in Neural Circuits. 2019 May 22;13.

69. Sorrenti V, Cecchetto C, Maschietto M, Fortinguerra S, Buriani A, Vassanelli S. Understanding the Effects of Anesthesia on Cortical Electrophysiological Recordings: A Scoping Review. International Journal of Molecular Sciences. 2021 Jan 28;22(3):1286.

70. Parel ST, Peña CJ. Genome-wide Signatures of Early-Life Stress: Influence of Sex. Biological Psychiatry. 2022 Jan;91(1):36–42.

71. Hill CA, Fitch RH. Sex Differences in Mechanisms and Outcome of Neonatal Hypoxia-Ischemia in Rodent Models: Implications for Sex-Specific Neuroprotection in Clinical Neonatal Practice. Neurology Research International. 2012;2012:1–9.

Figure legends

Figure 1. Oscillatory network activity in PL and BLAa of pre-juvenile and adolescent control mice. A, Diagram with timeline illustrating the experimental design. **B**, Digital photomontage of brightfield images with electrode tracts of the four-shank recording electrode and reconstruction of the 32 recording channels (blue dots) within **(i)** PL and IL or **(ii)** BLAa. **C, (i)** Extracellular LFP

1237 recording of oscillatory activity in PL, superficial layers II/III, of a male pre-juvenile mouse pup
1238 displayed after band pass filtering (3-6, 6-12, 12-100 Hz) and after 400 Hz high-pass filtering showing
1239 corresponding MUA activity. The color-coded frequency plot shows the wavelet spectra at identical
1240 time scale. Note the typical large-amplitude slow oscillations during urethane anaesthesia
1241 superimposed by theta, beta, and gamma band activity. Activity in the low-theta range (3-6 Hz) is
1242 particularly prominent. **(ii)** Same as C (i) for a male adolescent mouse pup. **D, (i)** Average logarithmic
1243 power spectra of prelimbic LFP in layers II/III (top) or layers V/VI (bottom) of male (left) and female
1244 (right) control (grey) or ELS (blue or magenta) pre-juvenile mice (males: N = 16-20/group, females:
1245 N = 13-18 /group). Note the broad peak in delta range (0.3-0.5 Hz) corresponding to slow-wave
1246 activity as well as the small peak in low-theta range at 4 Hz. **(ii)** Same as D (i) for adolescent control
1247 and ELS male and female mice (males: N = 13-16/group, females: N = 18-22/group). Note the shift
1248 of the peak in delta activity towards 1 Hz and the prominent broad peak in low theta activity (3-6 Hz).
1249 See Suppl. Table 2 for the exact number of pups per group in each graph in D. **E, (i)** Same as C (i)
1250 for corresponding oscillatory and MUA activity in the BLAa of a pre-juvenile male mouse pup. **(ii)**
1251 Same as C (ii) for corresponding oscillatory and MUA activity in the BLAa of an adolescent male
1252 mouse pup. Note the prominent activity in the theta range (3-6, 6-12 Hz). **F, (i)** Average logarithmic
1253 power spectra of the LFP in the BLAa of male (left) and female (right) control (grey) or ELS (blue or
1254 magenta) pre-juvenile mice (males, control: N = 13, ELS: N = 14, females, control: N = 12, ELS: N
1255 = 12). Note the peaks in theta range (3-5 and 6-8 Hz). **(ii)** Same as F (i) for adolescent control and
1256 ELS male and female mice (males, control: N = 12, ELS: N = 13, females, control: N = 13, ELS: N =
1257 17). Note the prominent broad peak in low theta activity (3-6 Hz).

1258 **Figure 2. ELS leads to hypercoupling within prelimbic-amygdala networks in male pre-**
1259 **juvenile mice. A,** Average coherence spectra of LFP in PL, layers II/III and LFP in BLAa (top) or
1260 LFP in PL, layers V/VI and LFP in BLAa (bottom) of male (left) and female (right) control (grey) or
1261 ELS (blue or magenta) pre-juvenile mice (males: N = 11-14/group, females: N = 10-11/group). Note
1262 the broad peak in coherence in the low-theta range (3-5 Hz) in all groups, which is particularly
1263 increased for coherence within PL layers II/III - BLAa networks in male ELS mice. **B,** Violin plots with

median and IQR showing the area under the curve (AUC) for coherence in the low-theta band (3-5 Hz) within prelimbic layer II/III - BLAa or prelimbic layer V/VI - BLAa networks in male (left) and female (right) control (grey) or ELS (blue or magenta) pre-juvenile mice. Note the significant increase in low theta coherence particularly within prelimbic layer II/III - BLAa networks in male pre-juvenile ELS mice. See Suppl. Table 3 for the exact number of pups per group in each graph. *p < 0.05, unpaired t-test.

Figure 3. ELS does not affect oscillatory coupling within adolescent prefrontal-amygdala networks. A, (i) Average coherence spectra of LFP in PL, layers II/III and LFP in BLAa, and corresponding violin plots with median and IQR showing the area under the curve (AUC) for coherence in the low-theta band (3-5 Hz) in adolescent control (grey, N = 9) and ELS (blue, N = 12) male mice. **(ii)** Same as A (i) for coherence between the LFP in PL, layers V/VI and BLAa (control, N = 11, ELS, N = 13). **B, (i)** Same as A (i) for adolescent control (grey, N = 11) and ELS (magenta, N = 15) female mice. **(ii)** Same as A (ii) for adolescent control (grey, N = 13) and ELS (magenta, N=17) female mice. **C, (i)**, Average coherence spectra between the LFP in PL, layers II/III and the LFP in BLAa for control pre-juvenile (light grey) and adolescent (dark grey) as well as ELS pre-juvenile (cyan) and adolescent (blue) male mice. The corresponding violin plots with median and IQR (right) show the fold change in low-theta coherence (3-5 Hz) between pre-juvenile and adolescent control (grey, N = 9) or pre-juvenile and adolescent ELS (blue, N = 12) male mice. Note that the fold increase in low-theta coherence is significantly smaller in ELS mice, suggesting that ELS promotes precocious development of functional interactions within these networks. **(ii)** Same as C (i) for coherence between the LFP in PL, layers V/VI and the LFP in BLAa (control: N = 11, ELS: N = 13). **D, (i)** Same as C (i) for female pre-juvenile (light grey) and adolescent (dark grey) control and pre-juvenile (orange) and adolescent (magenta) ELS mice. The corresponding violin plots with median and IQR (right) show the fold change in low-theta coherence (3-5 Hz) between pre-juvenile and adolescent control (grey, N = 11) or pre-juvenile and adolescent ELS (magenta, N = 15) female mice. **(ii)** Same as D (i) for coherence between the LFP in PL, layers V/VI and the LFP in BLAa (control: N = 13, ELS: N = 17). *p < 0.05, **p < 0.01, ***p < 0.001, unpaired t-test.

1291 **Figure 4. ELS increases the firing rates of a subpopulation of neurons in the BLAa in both**
1292 **male and female pre-juvenile mice and leads to a widespread increase in mean firing rates in**
1293 **BLAa of adolescent males**

1294 **A, (i)** Distribution and median (IQR) of instant firing rates (Hz) of single units in the BLAa in control
1295 (grey, n = 41 units from N = 12 pups) and ELS (blue, n = 36 units from N = 12 pups) male pre-juvenile
1296 mice. **(ii)**, Same as A (i) for Fano factor. **B**, Logarithmic frequency distribution (bin width 0.3 s) of
1297 firing rates of single units in BLAa from both control (grey, n = 41 units, left) and ELS (blue, n = 36
1298 units, right) pre-juvenile male mice. Note the bimodal distribution of firing rates in ELS mice,
1299 suggesting increased firing rates in a subpopulation of BLA neurons. **C, (i)** Distribution and mean ±
1300 SD of the mean valley-to-peak time (ms) corresponding to the mAHP of the extracellular action
1301 potential (see diagram above) of single units in BLAa in control (grey, n = 41 units) and ELS (blue,
1302 n=36 units) male pre-juvenile mice. Note the prominent decrease in ELS male mice. The diagram
1303 shows a representative action potential with key parameters highlighted in red. **(ii)** Same as C (i) for
1304 the full width at half maximum (FWHM, half-width (ms), see diagram in C (i)) of the extracellular
1305 action potential waveform. **D, (i)** Distribution and median (IQR) of instant firing rates (Hz) of single
1306 units in the BLAa in control (grey, n = 34 units from N = 9 pups) and ELS (magenta, n = 24 units
1307 from N = 10 pups) female pre-juvenile mice. **(ii)**, Same as C (i) for Fano factor. **E,** Logarithmic
1308 frequency distribution (bin width 0.3 s) of firing rates of single units in BLAa from both control (grey,
1309 n = 34 units, left) and ELS (magenta, n = 24 units, right) pre-juvenile female mice. Note the bimodal
1310 distribution of firing rates in ELS mice, suggesting increased firing rates in a subpopulation of BLA
1311 neurons. **F, (i)** Distribution and mean ± SD of the mean valley-to-peak time (ms) of single units in
1312 BLAa in control (grey, n = 36 units) and ELS (magenta, n = 24 units) female pre-juvenile mice. **(ii)**
1313 Same as F (i) for the full width at half maximum (ms) of the extracellular action potential waveform.
1314 ****p < 0.0001**,** Mann-Whitney test. **G, (i)** Distribution and median (IQR) of instant firing rates (Hz) of
1315 single units in the BLAa in control (grey, n = 47 units from N = 10 pups) and ELS (blue, n = 77 units
1316 from N = 11 pups) male adolescent mice. Mann-Whitney test, ***p = 0.0004. **(ii)**, Same as G (i) for
1317 Fano factor. Mann-Whitney test, **p = 0.0026. **H**, Logarithmic frequency distribution (bin width 0.3 s)

of firing rates of single units in BLAa from both control (grey, n = 47 units, left) and ELS (blue, n = 77 units, right) adolescent male mice. **I, (i)** Distribution and median (IQR) of the mean valley-to-peak time (ms) corresponding to the mAHP of the extracellular action potential of single units in BLAa in control (grey, n = 47 units) and ELS (blue, n = 77 units) male adolescent mice. Unpaired t-test, **p = 0.0041. **(ii)** Distribution and mean ± SD for the full width at half maximum (FWHM, half-width (ms), see diagram in C (i)) of the extracellular action potential waveform. **J, (i)** Distribution and median (IQR) of instant firing rates (Hz) of single units in the BLAa in control (grey, n = 109 units from N = 14 pups) and ELS (magenta, n = 29 units from N = 8 pups) female adolescent mice. **(ii)**, Same as J (i) for Fano factor. Mann-Whitney test, ****p < 0.0001. **K,** Logarithmic frequency distribution (bin width 0.3 s) of firing rates of single units in BLAa from both control (grey, n = 109 units, left) and ELS (magenta, n = 29 units, right) adolescent female mice. **L, (i)** Distribution and median (IQR) of the mean valley-to-peak time (ms) of single units in BLAa in control (grey, n = 109 units) and ELS (magenta, n = 29 units) female adolescent mice. Mann-Whitney test, *p = 0.0225 **(ii)** Distribution and mean ± SD of the full width at half maximum (ms) of the extracellular action potential waveform. Unpaired t test, ***p = 0.0006.

Figure 5. ELS causes chronic activation of BLAa neurons in both pre-juvenile males and females. A, (i) Representative photomicrograph images showing neurons immunopositive (+) for FosB (magenta, left) and PanFosB (green, center) in the BLAa of a control (top row) and ELS (bottom row) male P18 mouse. The merged images (right) show colocalization of FosB and PanFosB (white cells). Those PanFosB$^+$ cells that do not colocalize with FosB were identified as ΔFosB$^+$ (see arrowheads). **(ii)** Same as A (i) for a control and ELS female mouse. Scale bars: 50 µm. **B, (i)** Box and whisker plots of the number of ΔFosB$^+$ cells/mm^2 in the BLAa in control (grey) and ELS (blue) male mice at P14 and P18 (N = 5 mice/per group). Note the significant increase in ΔFosB$^+$ cells in male ELS mice at both time points. **(ii)** Bar diagrams showing the mean ± SEM of the number of ΔFosB$^+$ cells/mm^2 in either left (L) or right (R) hemisphere in the BLAa at P14 and P18 in control (grey) and ELS (cyan or blue) male mice (N = 3-5/group). Note that there is no significant difference between the hemispheres at either time point. **(iii)** Bar diagrams showing the mean ± SEM of the

1345 ΔFosB intensity of positive neurons in the BLAa at P14 and P18 in control (grey, N = 4-5/group) and
1346 ELS (cyan or blue, N = 5/group) male mice. Note that the ΔFosB intensity is similar in both treatment
1347 groups at both time points. **C, (i)** Same as B (i) for control (grey, N = 4-5/group) and ELS (red or
1348 magenta, N = 3-4/group) female mice. Note here that the effect of ELS is age-dependent, with no
1349 change by ELS in the number of $\Delta FosB^+$ cells/mm^2 at P14 but a strong significant increase by ELS
1350 at P18 in females. **(ii)** Same as B (ii) for control (grey, N = 3-5) and ELS (red or magenta, N = 3-4)
1351 female mice. Note that there is no significant difference between the hemispheres at either time
1352 point. **(iii)** Same as B (iii) in control (grey, N = 4-5/group) and ELS (red or magenta, N = 3-4/group)
1353 female mice. Note that the ΔFosB intensity is similar in both treatment groups at both time points. *p
1354 < 0.05, **$p < 0.01$, Two-way ANOVA with Sidak's post-hoc test.

1355 **Figure 6. ELS does not cause chronic activation of GABAergic pre-juvenile BLA neurons. A,**
1356 **(i)** Representative photomicrograph images showing neurons immunopositive (+) for FosB
1357 (magenta, left), PanFosB (cyan, left) and GAD67 (yellow, center) in the BLAa of a control (top row)
1358 and ELS (bottom row) male P18 mouse. The merged images on the left show $\Delta FosB^+$ cells (white
1359 arrowheads), i.e. those $PanFosB^+$ cells which do not colocalize with FosB. The merged image on
1360 the right shows that those $\Delta FosB^+$ cells (white arrowheads) do not colocalize with GAD67 (grey
1361 arrowheads) in the BLA. **(ii)** Same as (i) for a control and ELS female mouse. Note that while in
1362 males $\Delta FosB^+$ cells never colocalized with $GAD67^+$ cells, in both control and ELS females there was
1363 some colocalization with $GAD67^+$ cells (blue arrowheads). Scale bars: 50 µm. **B,** Box and whisker
1364 plots showing the number of $\Delta FosB^+$ cells/mm^2 (**i**, left), the number of $GAD67^+$ cells/mm^2 (**ii**, center)
1365 and double labelled $\Delta FosB^+$ and $GAD67^+$ cells/mm^2 (**iii**, right) in the BLAa in control (grey) and ELS
1366 (blue: male, magenta: female) mice at P18 (males: N = 5 mice per group, females: N = 4 mice per
1367 group). Note the trend towards an increase in $\Delta FosB^+$ cells after ELS in both sexes, which was close
1368 to statistical significance (Mann-Whitney test or paired t-test, respectively). Note that while the
1369 number of $GAD67^+$ cells is similar in all groups of mice, in control and ELS males $GAD67^+$ cells did
1370 never colocalize with $\Delta FosB^+$ cells. In both control and ELS females though, colocalization of $\Delta FosB^+$
1371 and $GAD67^+$ cells was present.

1372 **Figure 7. ELS decreases the firing activity of neurons in layers II/III of the prelimbic cortex in**
1373 **pre-juvenile males only. A, (i)** Distribution and median (IQR) of instant firing rates (Hz) of single
1374 units in PL in control (grey, n = 54 units from N = 12 pups) and ELS (blue, n = 90 units from N = 13
1375 pups) male pre-juvenile mice. Note the significant decrease in firing rates after ELS. **(ii)**, Same as A
1376 (i) for Fano factor. **B, (i)** Distribution and median (IQR) of the mean valley-to-peak time (ms)
1377 corresponding to the mAHP of the extracellular action potential of single units in the PL in control
1378 (grey, n = 54 units) and ELS (blue, n = 90 units) male pre-juvenile mice. **(ii)** Same as B (i) for the full
1379 width at half maximum (ms) of the extracellular action potential waveform. **C, (i)** Distribution and
1380 median (IQR) of instant firing rates (Hz) of single units in PL in control (grey, n = 74 units from N =
1381 13 pups) and ELS (magenta, n = 49 units from N = 10 pups) female pre-juvenile mice. **(ii)**, Same as
1382 C (i) for Fano factor. **D, (i)** Distribution and median (IQR) of the mean valley-to-peak time (ms) of
1383 single units in the PL in control (grey, n = 74 units) and ELS (magenta, n = 49 units) female pre-
1384 juvenile mice. **(ii)** Same as D (i) for the full width at half maximum (ms) of the extracellular action
1385 potential waveform. Note the significant increase in half-width after ELS. *$p < 0.05$, ***$p < 0.001$***,***
1386 Mann-Whitney test.

1387 **Figure 8. ELS affects the locking of spikes to the low-theta rhythm within prefrontal-amygdala**
1388 **networks. A, (i)** Top: Polar plots showing the probability distribution of the preferred BLAa spike
1389 phase locked to the 3-5 Hz LFP within the BLAa itself, for control (left, grey) and ELS (right, blue)
1390 male pre-juvenile mice. Red arrows show the vector mean phase for each group, and their length
1391 was scaled to match the height of the tallest bin. 0° corresponds to the peak of the theta cycle, and
1392 180° to its through. Bottom: comparison of the mean vector length for each unit (left) and the relative
1393 proportion of locked (solid colors) and non-locked (striped pattern) units within each group (right).
1394 **(ii)** Same as A (i) for female control (left, grey) and ELS (right, magenta) pre-juvenile mice. **(iii)** Same
1395 as A (i) for PL spikes phase locked to the 3-5 Hz LFP within the PL itself, for control (left, grey) and
1396 ELS (right, blue) pre-juvenile male mice. **(iv)** Same as A (iii) for female control (left, grey) and ELS
1397 (right, magenta) pre-juvenile mice. **B, (i)** Top: Polar plots showing the probability distribution of the
1398 preferred BLAa spike phase locked to the 3-5 Hz LFP of the PL, for control (left, grey) and ELS (right,

1399 blue) male pre-juvenile mice. Red arrows show the vector mean phase for each group, and their
1400 length was scaled to match the height of the tallest bin. Bottom: comparison of the mean vector
1401 length for each unit (left) and the relative proportion of locked (solid colors) and non-locked (striped
1402 pattern) units within each group (right). **(ii)** Same as B (i) for female control (left, grey) and ELS (right,
1403 magenta) pre-juvenile mice. **(iii)** Same as B (i) for PL spikes phase locked to the 3-5 Hz LFP of the
1404 BLAa, for control (left, grey) and ELS (right, blue) pre-juvenile male mice. **(iv)** Same as B (iii) for
1405 female control (left, grey) and ELS (right, magenta) pre-juvenile mice. **$p < 0.01$, Mann-Whitney test.

1406 **Figure 9. Summary of the sex-dependent effects of ELS on pre-juvenile prefrontal-amygdala**
1407 **networks.** Diagram showing baseline neuronal firing activity as well as functional interactions
1408 within juvenile prefrontal-amygdala networks in controls (top) and after ELS in male (bottom left) or
1409 female (bottom right) pups.

1410

Figure 1

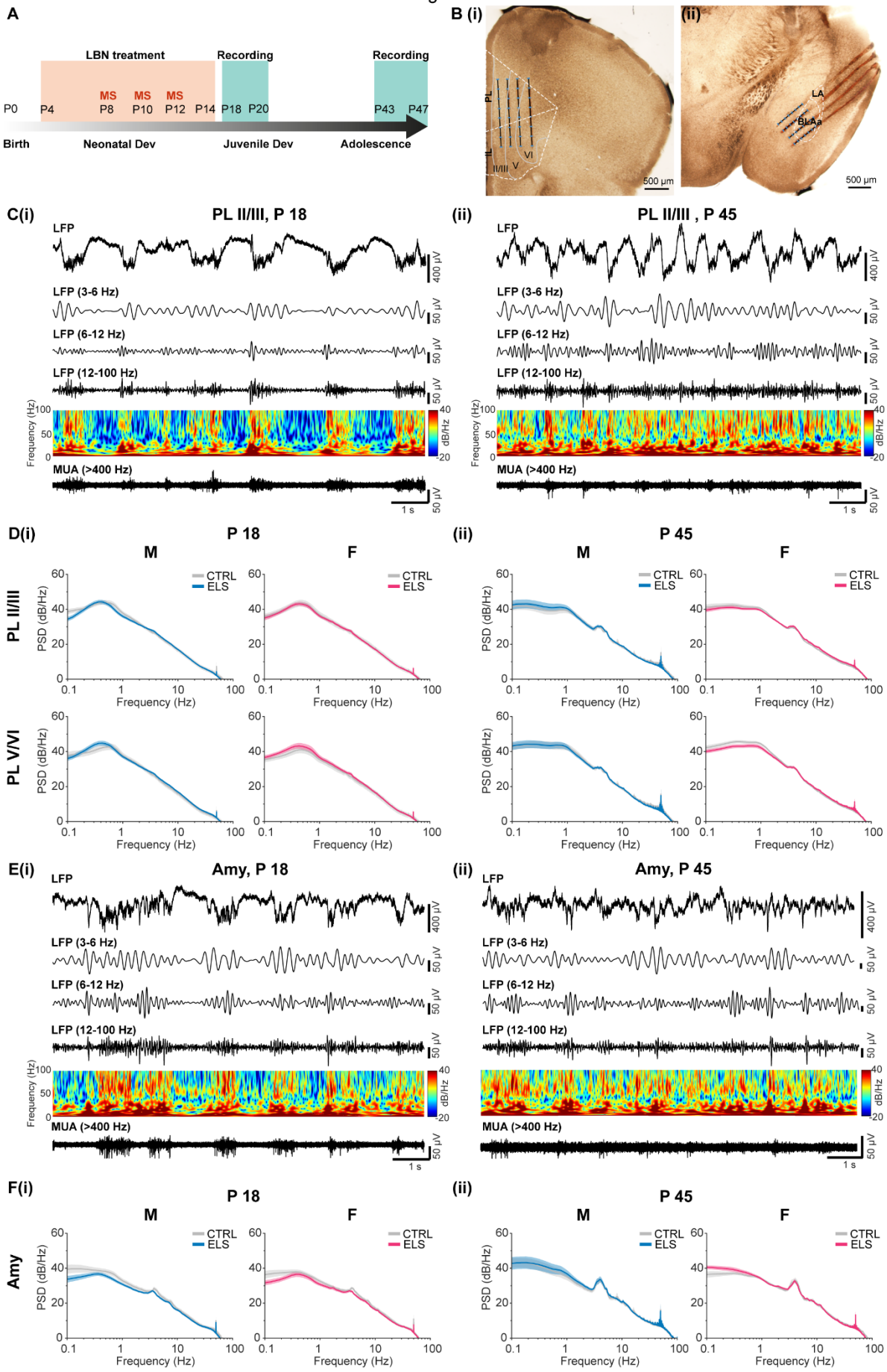
A
LBN treatment
Recording
Recording
MS
MS
MS
P0
P4
P8
P10
P12
P14
P18
P20
P43
P47
Birth
Neonatal Dev
Juvenile Dev
Adolescence
B (i)
(ii)
PL
IL
II/III
V
VI
LA
BLA
500 µm
500 µm
C(i)
PL II/III, P 18
(ii)
PL II/III , P 45
LFP
LFP (3-6 Hz)
LFP (6-12 Hz)
LFP (12-100 Hz)
MUA (>400 Hz)
400 µV
50 µV
1 s
Frequency (Hz)
dB/Hz
D(i)
P 18
(ii)
P 45
M
F
PL II/III
PL V/VI
CTRL
ELS
PSD (dB/Hz)
Frequency (Hz)
E(i)
Amy, P 18
(ii)
Amy, P 45
F(i)
P 18
(ii)
P 45
Amy

Figure 2

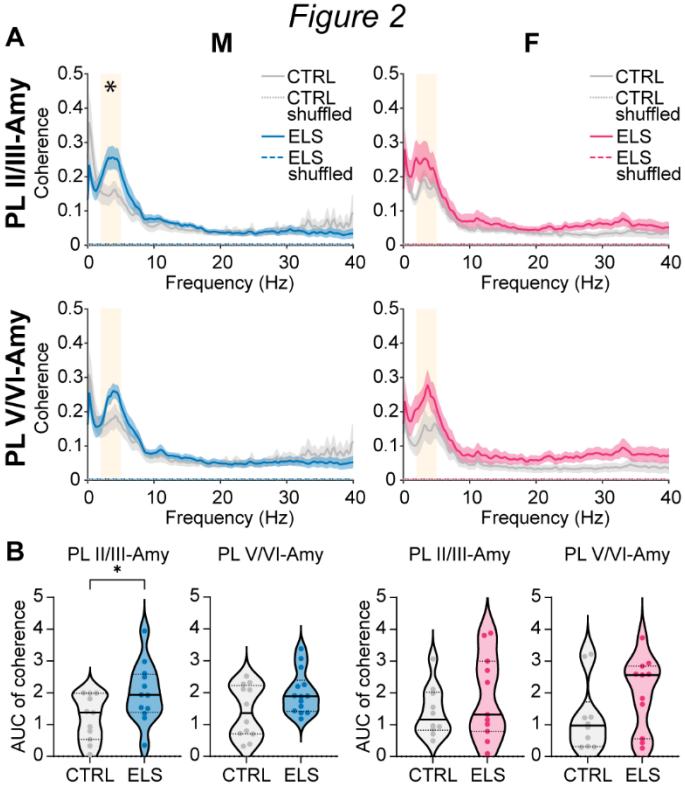
A
M
F
PL II/III-Amy
PL V/VI-Amy
Coherence
Frequency (Hz)
CTRL
CTRL shuffled
ELS
ELS shuffled
*
B
PL II/III-Amy
PL V/VI-Amy
AUC of coherence
CTRL
ELS

Figure 3

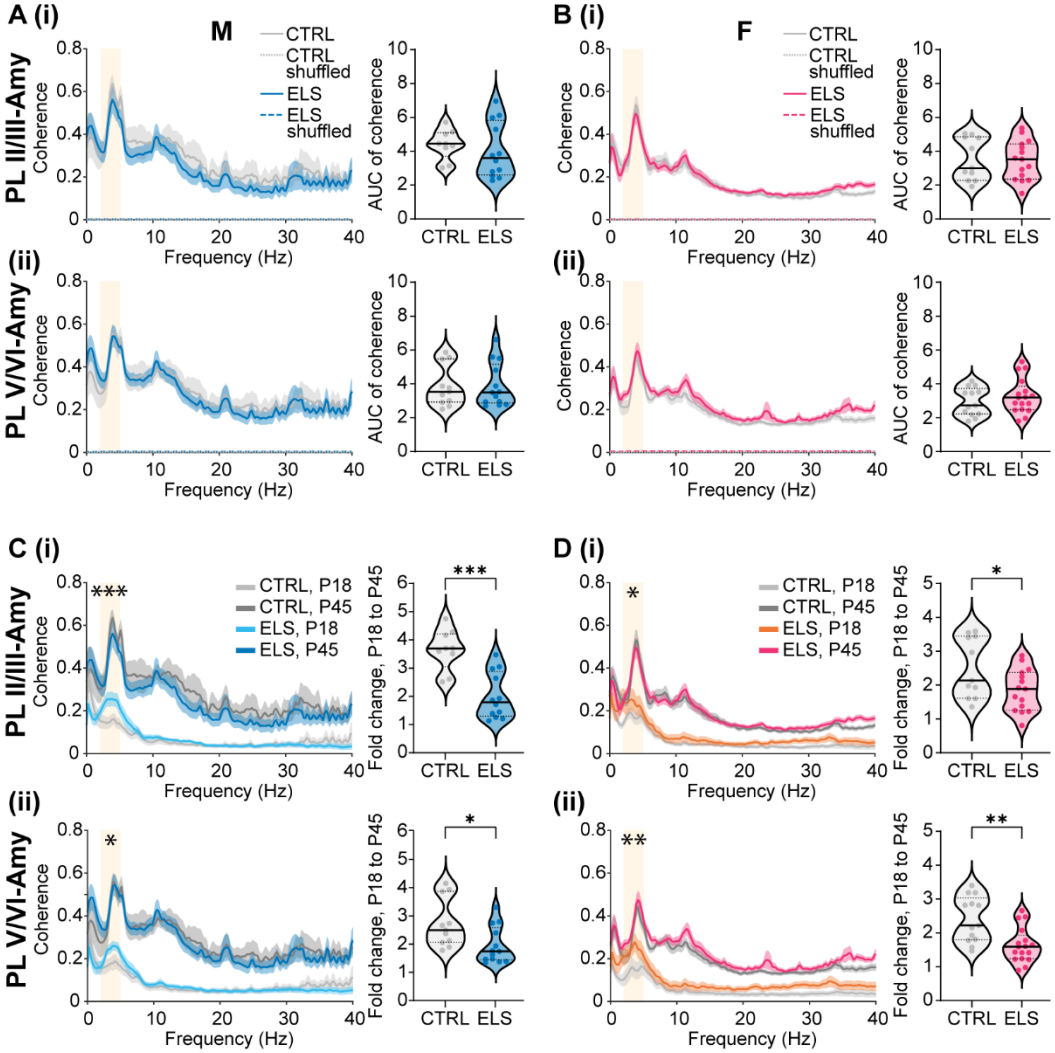
A (i)
M
CTRL
CTRL shuffled
ELS
ELS shuffled
PL II/III-Amy
Coherence
Frequency (Hz)
AUC of coherence
CTRL ELS
(ii)
PL V/VI-Amy
B (i)
F
(ii)
C (i)
CTRL, P18
CTRL, P45
ELS, P18
ELS, P45
***
Fold change, P18 to P45
(ii)
*
D (i)
(ii)
**

Figure 4

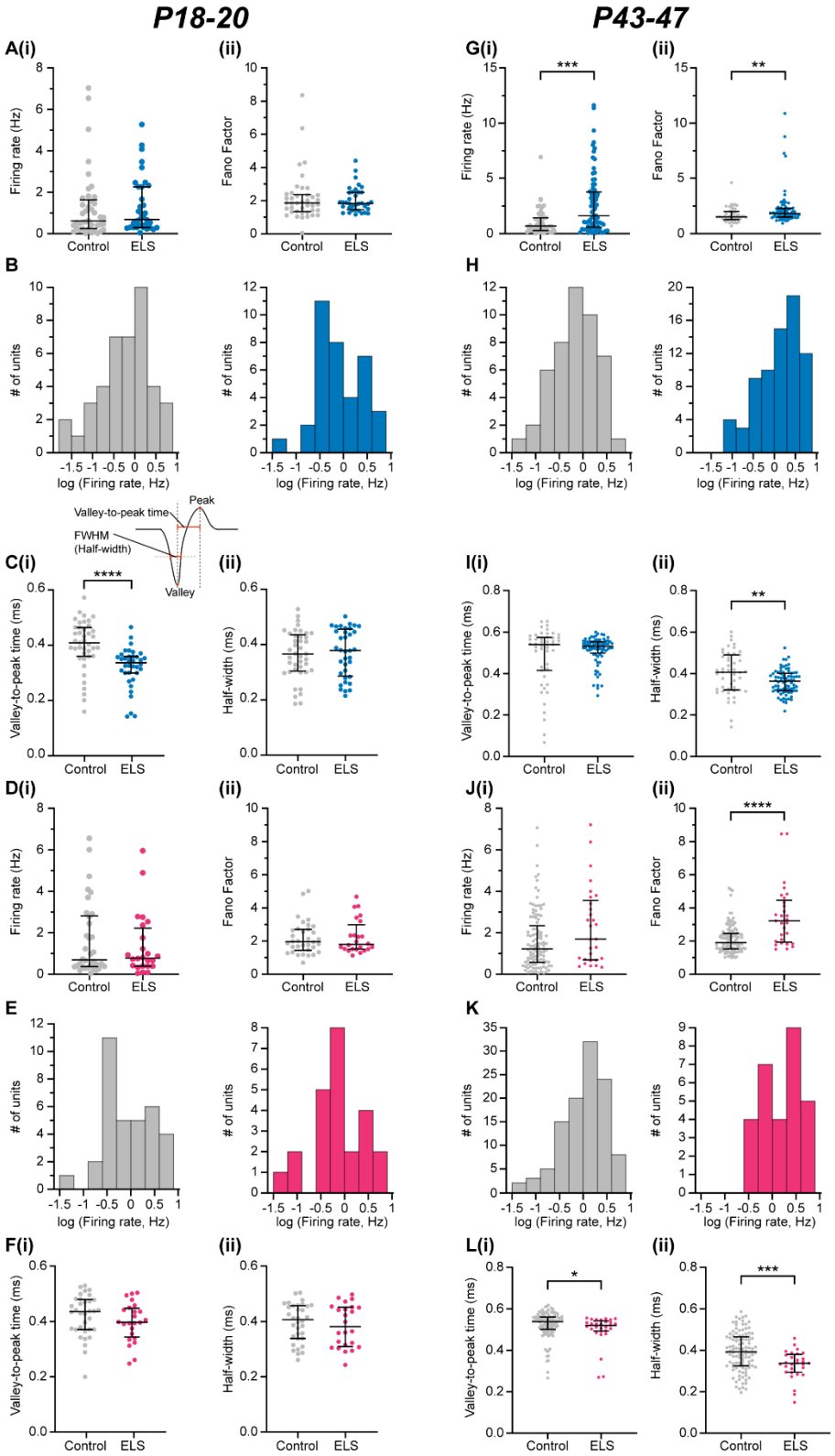
P18-20
P43-47
A(i)
(ii)
G(i)
(ii)
Firing rate (Hz)
Fano Factor
Control
ELS
***
**
B
H
# of units
log (Firing rate, Hz)
Valley-to-peak time
Peak
FWHM
(Half-width)
Valley
C(i)
(ii)
I(i)
(ii)
****
**
Valley-to-peak time (ms)
Half-width (ms)
D(i)
(ii)
J(i)
(ii)
****
E
K
F(i)
(ii)
L(i)
(ii)
*
***

Figure 5

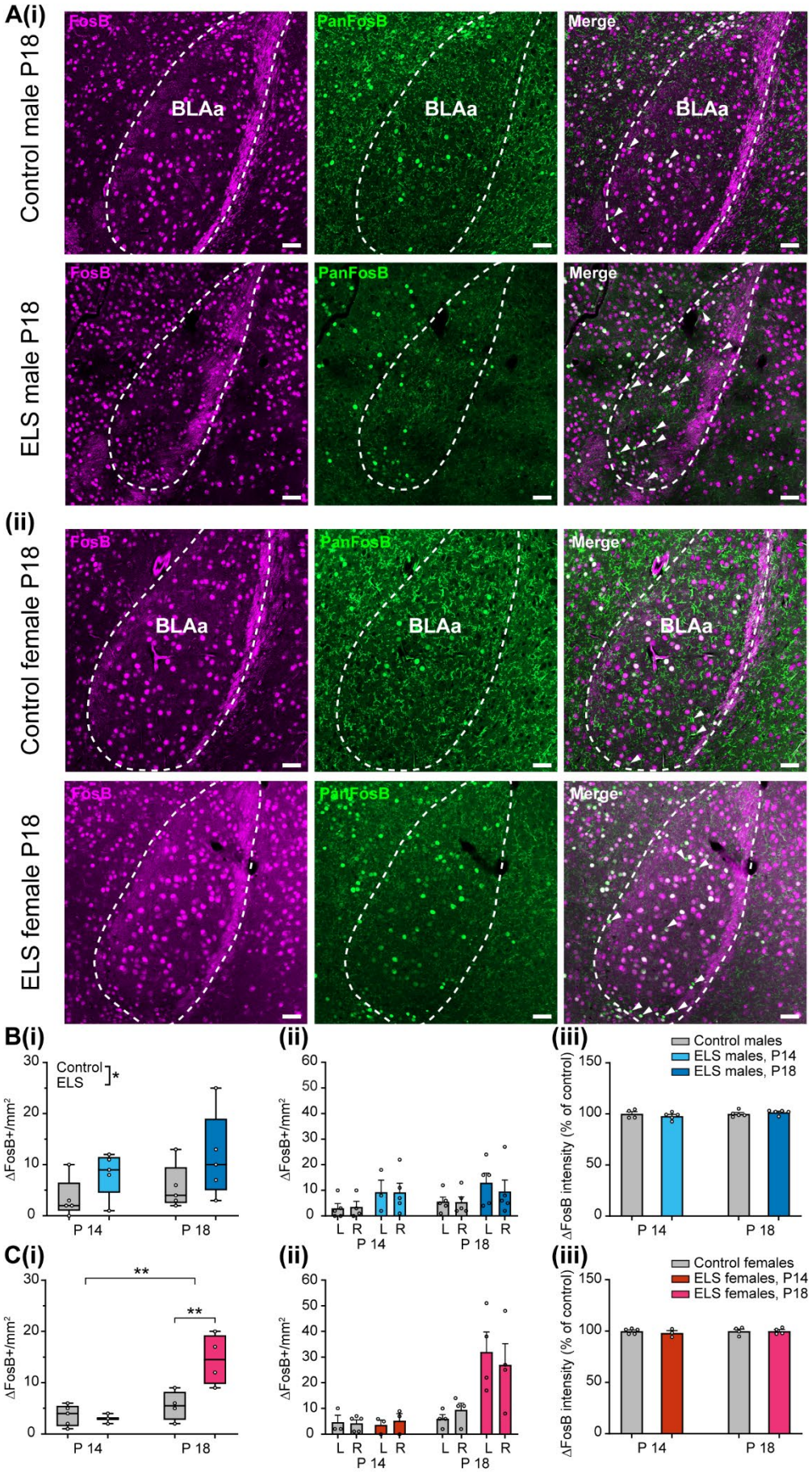
A(i)
Control male P18
ELS male P18
(ii)
Control female P18
ELS female P18
FosB
PanFosB
Merge
BLAa
B(i)
Control
ELS
*
ΔFosB+/mm²
P 14
P 18
(ii)
L R L R
(iii)
Control males
ELS males, P14
ELS males, P18
ΔFosB intensity (% of control)
C(i)
**
(ii)
(iii)
Control females
ELS females, P14
ELS females, P18

Figure 6

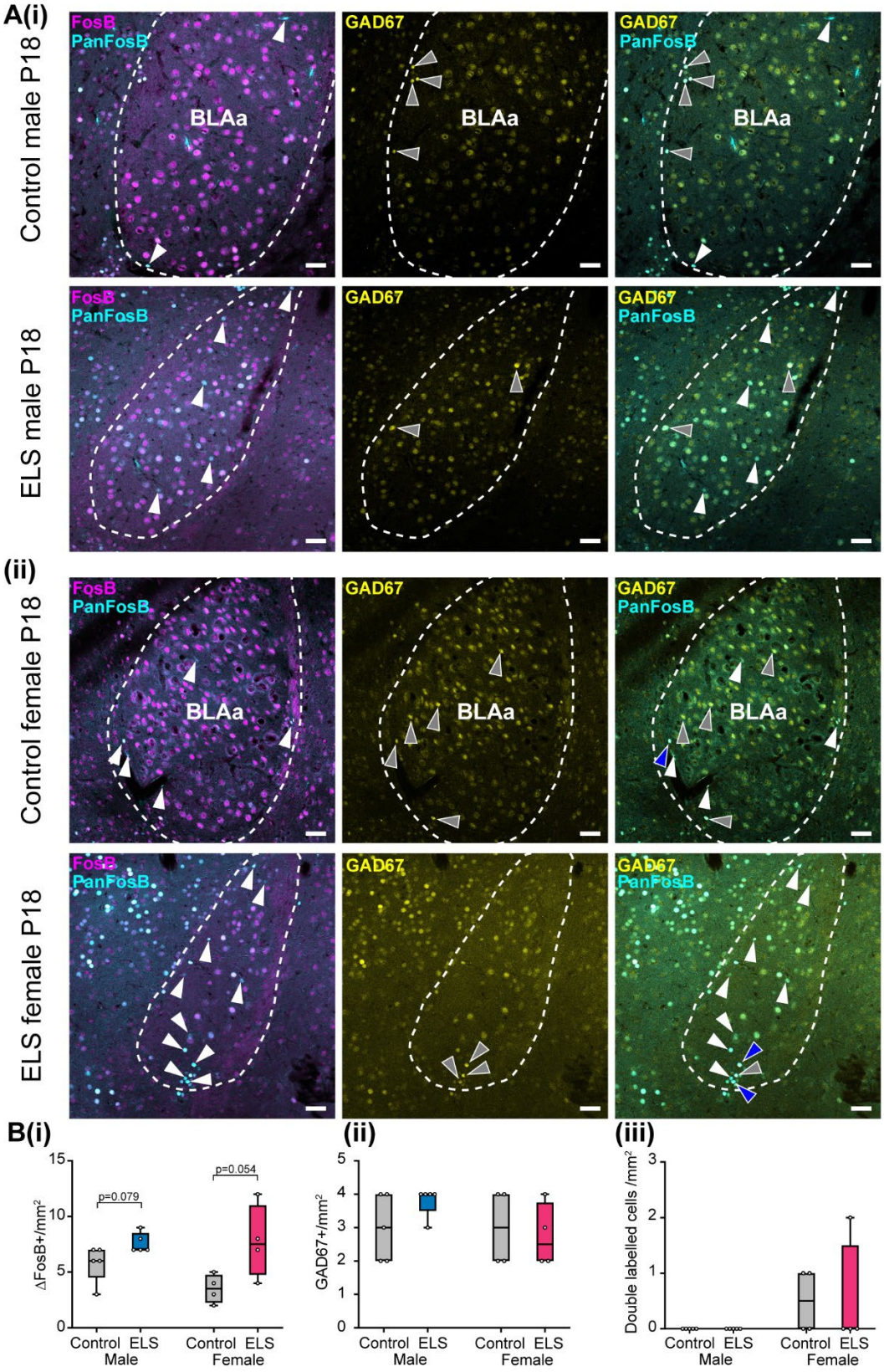
A(i)
Control male P18
ELS male P18
(ii)
Control female P18
ELS female P18
FosB
PanFosB
GAD67
BLAa
B(i)
(ii)
(iii)
ΔFosB+/mm²
p=0.079
p=0.054
GAD67+/mm²
Double labelled cells /mm²
Control
ELS
Male
Female

Figure 7

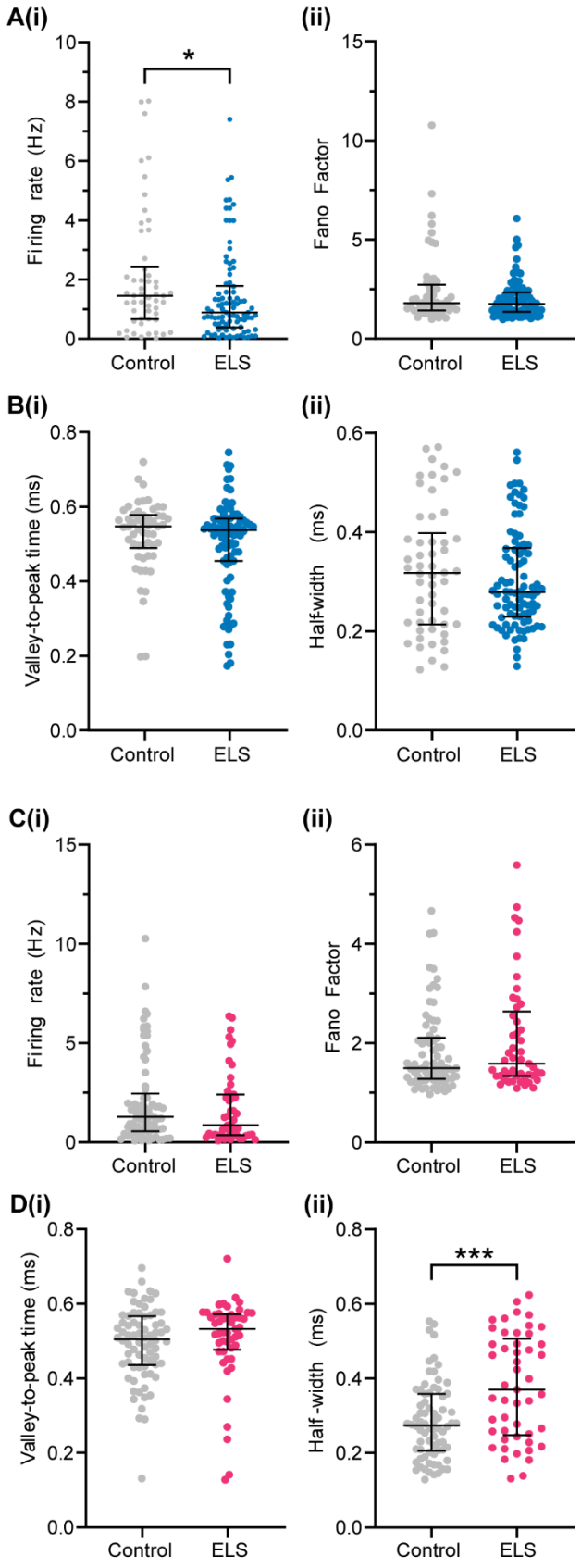
A(i)
(ii)
Firing rate (Hz)
Fano Factor
*
Control
ELS
B(i)
(ii)
Valley-to-peak time (ms)
Halfwidth (ms)
C(i)
(ii)
D(i)
(ii)
Half-width (ms)
***

Figure 8

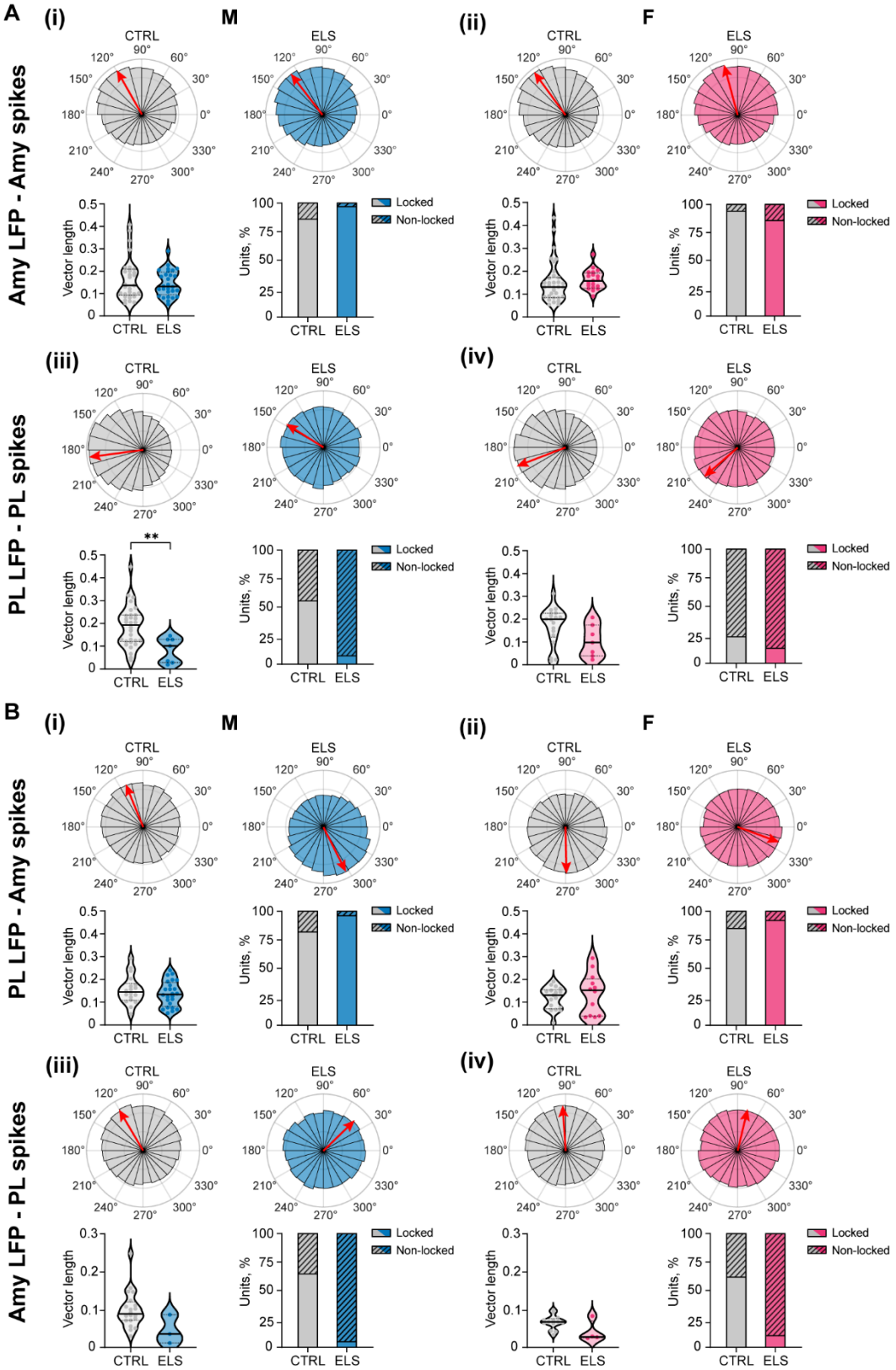
A
(i)
M
(ii)
F
Amy LFP - Amy spikes
(iii)
(iv)
PL LFP - PL spikes
B
PL LFP - Amy spikes
Amy LFP - PL spikes
CTRL
ELS
Vector length
Units, %
Locked
Non-locked
**

Figure 9

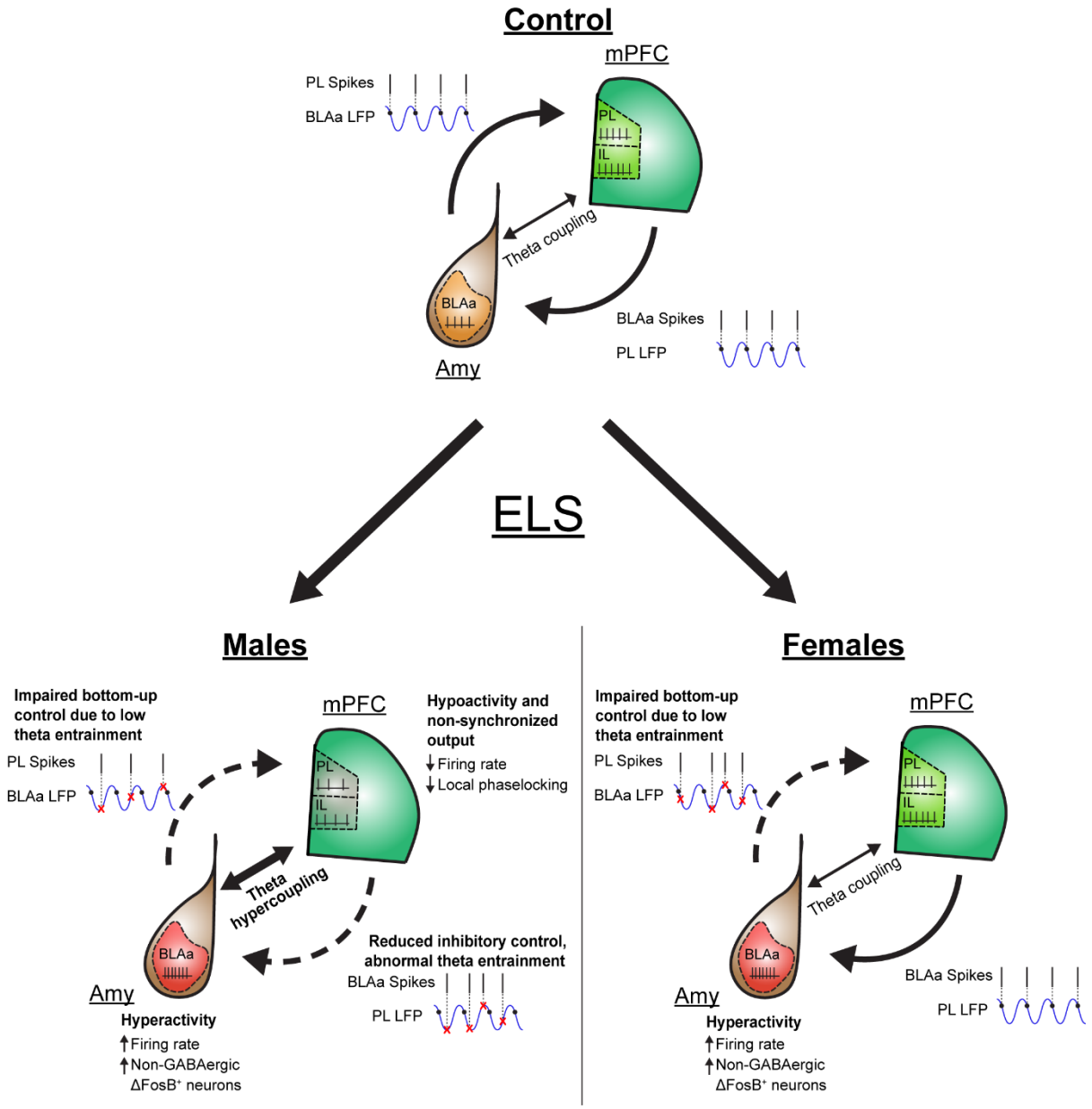
Control
mPFC
PL Spikes
BLAa LFP
PL
IL
Theta coupling
BLAa
Amy
BLAa Spikes
PL LFP
ELS
Males
Impaired bottom-up control due to low theta entrainment
PL Spikes
BLAa LFP
mPFC
Hypoactivity and non-synchronized output
↓Firing rate
↓Local phaselocking
Theta hypercoupling
Reduced inhibitory control, abnormal theta entrainment
BLAa Spikes
PL LFP
Amy
Hyperactivity
↑Firing rate
↑Non-GABAergic ΔFosB⁺ neurons
Females
Impaired bottom-up control due to low theta entrainment
PL Spikes
BLAa LFP
mPFC
Theta coupling
BLAa Spikes
PL LFP
Amy
Hyperactivity
↑Firing rate
↑Non-GABAergic ΔFosB⁺ neurons